

Gravitational Recoil during Binary Black Hole Coalescence using the Effective One Body Approach

Thibault Damour¹ and Achamveedu Gopakumar²

¹ *Institut des Hautes Etudes Scientifiques, 91440 Bures-sur-Yvette, France*

² *Theoretisch-Physikalisches Institut, Friedrich-Schiller-Universität,
Max-Wien-Platz 1, 07743 Jena, Germany*

(Dated: October 3, 2018)

Abstract

During the coalescence of binary black holes, gravitational waves carry linear momentum away from the source, which results in the recoil of the center of mass. Using the Effective One Body approach, that includes nonperturbative resummed estimates for the damping and conservative parts of the compact binary dynamics, we compute the recoil during the late inspiral and the subsequent plunge of non-spinning black holes of comparable masses moving in quasi-circular orbits. Further, using a prescription that smoothly connects the plunge phase to a perturbed single black hole, we obtain an estimate for the total recoil associated with the binary black hole coalescence. We show that the crucial physical feature which determines the magnitude of the terminal recoil is the presence of a “burst” of linear momentum flux emitted slightly before coalescence. When using the most natural expression for the linear momentum flux during the plunge, together with a Taylor-expanded $(v/c)^4$ correction factor, we find that the maximum value of the terminal recoil is ~ 74 km/s and occurs for $\eta = \frac{m_1 m_2}{(m_1 + m_2)^2} \simeq 0.2$, i.e., for a mass ratio $m_2/m_1 \simeq 0.38$. Away from this optimal mass ratio, the recoil velocity decreases approximately proportionally to the scaling function $\tilde{f}(\eta) = \eta^2 (1 - 4\eta)^{1/2} (1.0912 - 1.04\eta + 2.92\eta^2)$. We comment, however, on the fact that the above ‘best bet estimate’ is subject to strong uncertainties because the location and amplitude of the crucial peak of linear momentum flux happens at a moment during the plunge where most of the simplifying analytical assumptions underlying the Effective One Body approach are no longer justified. Changing the analytical way of estimating the linear momentum flux, we find maximum recoils that range between 49 and 172 km/s.

PACS numbers: 04.30Db, 04.25.Nx, 04.80.Nn, 95.55.Ym

I. INTRODUCTION

During the coalescence of compact binaries, along with energy and angular momentum, the system radiates linear momentum. The loss of linear momentum via gravitational radiation results in the recoil of the center of mass of the binary. It is astrophysically important and desirable to obtain a dependable estimate for the velocity of the center of mass of comparable-mass black hole binaries undergoing coalescence [1, 2]. Notably, in models of massive black hole formation involving successive mergers, recoils large enough to eject coalescing black holes from dwarf galaxies or globular clusters would effectively terminate the process. This motivation has recently led several authors to estimate the recoil velocity of coalescing black hole binaries by means of various methods [3, 4, 5]. Ref. [3] employed black hole perturbation theory to describe the motion of a test mass moving in a black hole background, i.e., the case where the symmetric mass ratio $\eta = \frac{m_1 m_2}{(m_1 + m_2)^2} \ll 1$. They combined a numerical estimate of the recoil velocity up to the Last Stable Orbit (LSO), with two crude estimates for the recoil acquired during the subsequent plunge phase. Then they assumed that their test-mass estimates could be proportionally scaled up to the comparable-mass cases ($4\eta \sim 1$) with the function

$$f(\eta) = \eta^2 \sqrt{1 - 4\eta}, \quad (1)$$

which appears as an overall factor in the leading (“Newtonian”) analytical estimate of the recoil, as first computed in Ref. [6]. The final estimates of Ref. [3] range (for non-spinning black holes) between a lower value $\sim 54 (f(\eta)/f_{\max})$ km/s and an upper one $\sim 465 (f(\eta)/f_{\max})$ km/s, where $f_{\max} = f(\eta_{\max}) = f(0.2) = 0.0178885$. Another set of estimates was obtained from an approach that employs a mixture of numerical relativity and black hole perturbation theory for the merger of comparable mass non-spinning black holes [4]. In particular, for a mass ratio $m_2/m_1 = 0.5$, corresponding to a value $\eta = 0.2222$, close to the value $\eta_{\max} = 0.2$, where $f(\eta)$, given by Eq. (1), reaches its maximum value [$f(0.2222)/f(0.2) = 0.01646/0.01789 \simeq 0.92$], Ref. [4] estimates a recoil velocity $\sim 250 \pm 150$ km/s. Finally, using an analytical estimate, which is further discussed below, a maximum recoil (reached for $\eta \sim 0.2$) equal to 250 ± 50 km/s was obtained in Ref. [5].

Summarizing, the recent estimates are consistent with a maximum recoil velocity ~ 250 km/s for non-spinning black holes [3, 4, 5]. In contrast, we shall estimate here, by using the Effective One Body (EOB) approach to binary black hole dynamics, detailed in

Refs. [7, 8, 9, 10, 11], that the maximum recoil velocity for non-spinning coalescing black holes is probably significantly smaller, and of the order $\sim 50 - 74$ km/s. However, we shall conclude that this estimate is rather uncertain because it depends on a specific way of describing the linear momentum flux during a crucial phase of the plunge which is (mildly) relativistic, and has not been yet analytically studied in detail. When changing our preferred assumptions for describing the linear momentum flux, we find maximal recoil velocities that vary in the range $49 - 172$ km/s.

Let us recall that the coalescence of isolated black hole binaries may be viewed as consisting of the following three phases. The first phase is that of gravitational-radiation-driven slow inspiral in quasi-circular orbits. This leads, after a very long period of adiabatic shrinkage of the orbital separation, to the binary approaching its LSO. At the LSO, the inspiral phase changes to some sort of plunge, dominated by general relativistic strong-field effects. This plunge phase results in the merger of the two black holes and the dynamics of the final black hole, thus formed, may be described in terms of black hole quasi-normal modes.

During the early inspiral, the dynamics of compact binaries can be described very accurately by the post-Newtonian (PN) approximation to general relativity. The PN approximation to general relativity allows one to express the equations of motion for a compact binary as corrections to Newtonian equations of motion in powers of $(v/c)^2 \sim GM/(c^2 R)$, where v , M , and R are the characteristic orbital velocity, the total mass and the typical orbital separation of the binary respectively. For a compact binary, treated to consist of non-spinning point masses, of arbitrary mass ratio $\eta = \frac{m_1 m_2}{M^2}$, where m_1 and m_2 are the masses of the components and $M = m_1 + m_2$, the leading “Newtonian” contribution ¹ to linear momentum flux $\mathcal{F}_{\mathbf{P}}^i$ and the associated instantaneous recoil $\mathbf{v}_{\text{com}}^i$, i.e., the instantaneous velocity of center of mass can be derived from the investigations that dealt either with wave-zone flux computations, or with near-zone radiation-reaction ones [12, 13, 14, 15]. This allowed Ref. [6] to derive the following explicit leading order results (for a circularized orbit of radius R)

$$|\mathcal{F}_{\mathbf{P}}^i| = \frac{464 c^4}{105 G} f(\eta) \left(\frac{G M}{c^2 R} \right)^{11/2}, \quad (2a)$$

¹ Or rather “quasi-Newtonian”, as this leading contribution corresponds to 3.5PN $\mathcal{O}(v^7/c^7)$ radiation reaction terms in the equations of motion for the binary.

$$\left| \frac{v_{\text{com}}^i}{c} \right| = \frac{464}{105} f(\eta) \left(\frac{GM}{c^2 R} \right)^4. \quad (2b)$$

where $f(\eta)$ denotes the combination introduced in Eq. (1). The function $f(\eta)$ vanishes both in the limit of extreme mass ratio (test-mass limit, $\eta \rightarrow 0$), and in the case of equal mass binaries ($\eta = 1/4$). It reaches the maximum value $f_{\text{max}} = 0.0178885$ for $\eta_{\text{max}} = 0.2$, corresponding to a mass ratio $m_2/m_1 = (3 \pm \sqrt{5})/2 \sim 0.3820$ or 2.618 . In the following, we shall generally (though not systematically) employ units where $G = c = 1$.

The above leading-order results do not allow one to reliably estimate the final recoil of a coalescing binary black hole. Indeed, on the one hand they neglect higher-order PN corrections that might become fractionally large near the LSO and during the subsequent plunge, and on the other hand, they do not take into account the crucial transition between quasi-circular inspiral and plunge. As exemplified by previous works [3, 4, 5, 16], one can think of several different ways of going beyond the above results, given by Eqs. (2). As first attempted by Detweiler and Fitchett [16], one can use perturbation theory around black hole backgrounds to calculate the linear momentum flux emitted by a test particle moving around a black hole, assuming then a scaling proportional to $f(\eta)$ in order to go from the test-mass case ($\eta \ll 1$) to the comparable-mass one. Ref. [16] considered only circular motions (both above and below LSO), while Ref. [3] combined information about circular orbits above the LSO with crude estimates of the linear momentum flux during the plunge following the LSO crossing. However, we note that this approach is yet to be applied for the relevant case of (non-geodesic) plunging motions. The Lazarus program, which employs a mixture of perturbation theory and numerical relativity, to study the late inspiral and the merger of black hole binaries is not limited to the case $\eta \ll 1$. However, these simulations are limited to rather short evolution time spans. For instance, Ref. [4] mentions that the simulations are accurate only for “less than $15 M$ in time”, which is significantly smaller than the 3PN-accurate estimate of the orbital period of a comparable-mass black hole binary at the LSO: $T_{\text{LSO}}^{3\text{PN}} \simeq 71.2 M$ [9]. This forces state-of-the-art numerical simulations to employ initial data sets where the two holes are already quite near to each other (and, in fact, probably closer than the LSO). It is indeed a challenge to construct initial data sets for tight black hole binaries, and which do correspond to the physically correct “no-incoming radiation” criteria. [See Refs. [17, 18] for prescriptions to construct ‘realistic initial data sets’.] Presence of spurious radiation in the initial data sets is likely to dominate

and thereby invalidate the estimate of the linear momentum flux. However, a comparison between numerically constructed initial data sets and analytically determined characteristics of tight binary systems, performed in Ref. [19], have indicated the ability of the Effective One Body (EOB) approach [7, 9, 10] to describe rather accurately the initial data obtained by the helical Killing vector method [20], which is carefully aimed at minimizing the amount of spurious radiation present in the initial state.

In view of the above situation, we consider that our present “best bet” for obtaining a dependable estimate for the gravitational recoil during the late inspiral and plunge phases of a black hole binary consists in employing the EOB approach. This approach has already been used to compute complete gravitational waveforms emitted during the inspiral and merger of (non-spinning and spinning) black holes [8, 11]. As first proposed in Ref. [8], this is achieved by considering the waveform emitted by the binary beyond the LSO, through the subsequent “plunge”, down to, approximately, the “light ring” ($R \simeq 3M$), and by matching it there to a “ring down” signal constructed using the quasi-normal modes of the resultant final black hole. As this (extended) EOB approach will be central to the present paper, let us recall the main arguments of Ref. [8] for proposing the apparently bold strategy of analytically describing the plunge beyond the LSO, down to $R \simeq 3M$. A first argument is that the EOB approach is a resummation technique which was carefully devised to work not with the usually considered, badly convergent, PN-expanded equations of motion or flux quantities, but instead with a (EOB) re-summed Hamiltonian and a (Padé) re-summed damping force showing no sign of bad behavior during most of the “plunge”. In particular, it was found in Ref. [8] that the word “plunge” to qualify the dynamics beyond the LSO is a misnomer, and that this phase is better thought of as being still a quasi-circular inspiral motion, even down to the light ring $R \simeq 3M$. Indeed, it was found that the quasi-circularity condition ($\dot{R} \ll R\dot{\varphi}$) remains satisfied with good accuracy beyond the LSO, down to $R \simeq 3M$. This is illustrated in Fig. 1 which shows (for $\eta = 0.2$) the evolution of the “azimuthal” ($g^{\varphi\varphi}p_\varphi^2$) and “radial” ($g^{RR}p_R^2$) kinetic energies during the plunge down to the light-ring, $R \simeq 3M$. The crucial point is that the ratio $\mathcal{R} \equiv g^{RR}p_R^2/g^{\varphi\varphi}p_\varphi^2$ stays significantly smaller than one during the entire plunge. Its value at $R \simeq 3M$ is $\mathcal{R}_{\text{light-ring}} \simeq 0.281$.

As for the idea of matching the gravitational wave emission to a quasi-normal-mode (QNM) “ring-down” signal around $R \simeq 3M$, let us recall that it was realized long ago that the basic physical reason underlying the presence of a QNM-type merger signal, that ends

the plunge signal, was that the $l \geq 2$ gravitational waves emitted by the collapsing system are strongly filtered by the potential barrier, centered around $R \simeq 3M$, describing the radial propagation of the gravitational waves [21, 22, 23]².

Recently, Blanchet, Qusailah and Will [5] have employed an ‘‘approximation’’ to the EOB method in the sense that they ‘assume that the plunge can be viewed as that of a ‘‘test particle’’ of mass $\mu = \frac{m_1 m_2}{M}$ moving in the fixed Schwarzschild geometry of a body of mass M ’. They also assumed that the effect of radiation reaction damping on the plunge orbit may be ignored. They then matched, in various ways, a circular orbit at the Schwarzschild LSO, i.e., $6M$, to a suitable plunge orbit. By contrast, we shall use here the *full EOB* approach [8], which does not need to ‘assume’ that the plunge can be viewed as that of suitable test particle, but instead proves it [see Refs. [7, 8, 9]], and which does not need to match a circular orbit to a plunge orbit at the LSO, because it automatically embodies a *smooth transition* between the ‘inspiral’ and the ‘plunge’. Let us also note that the ‘effective test body’ used in the EOB method does not evolve in a fixed Schwarzschild geometry of mass M , but instead in a deformed Schwarzschild background, whose geometry was algorithmically derived to 2PN accuracy in Ref. [7], and to 3PN order in Ref. [9] [see also Ref. [10] for the incorporation of spin effects]. In addition, while Ref. [5] formally let their ‘test particle’ fall down to the horizon at $R = 2M$, an important ingredient of our approach will be to match the plunge signal to a QNM-based ring-down one at $R \simeq 3M$.

On the other hand, an important result of Ref. [5] concerns the higher-order PN corrections to the ‘Newtonian’ linear momentum flux, given by Eq. (2). Using the multi-polar post-Minkowskian approach [24, 25, 26, 27, 28, 29], and its higher-order implementations [30, 31, 32], Ref. [5] has gone beyond the previous 1PN-accurate studies of recoil effects, available in Ref. [33], by including both the 1.5PN order ‘tail’ contribution and the next 2PN order corrections. Ref. [5] finds that the linear momentum flux at infinity, for binary systems in *circular orbits*, is given by a PN expansion of the form

$$\mathcal{F}_{\mathbf{P}}^{i(\text{BQW})} = -\frac{464}{105} f(\eta) v_{\omega}^{11} F(v_{\omega}; \eta) \lambda^i, \quad (3)$$

² For the test-particle case, this follows from the explicit form of the Regge-Wheeler-Zerilli effective potentials. In the comparable-mass case, we must contemplate the $l \geq 2$ binary gravitational wave signal as propagating in the spacetime generated by the binary system, and approximate the latter (when the two holes are closer than $3M$, and when considering the waves propagating in the domain $R \geq 3M$) by the external geometry of a single hole (of mass-energy $\simeq M$).

where $f(\eta)$ is given by Eq. (1) above ³, and

$$v_\omega \equiv (M \Omega)^{1/3}, \quad (4)$$

with $\Omega \equiv d\varphi/dT$ denoting the orbital angular velocity. The factor $F(v_\omega; \eta)$ yields the 2PN-accurate ‘‘Taylor-expanded’’ PN-corrections to the linear momentum flux (when the latter is expressed in terms of the above defined v_ω) and it reads

$$F(v_\omega; \eta) = 1 + F_2(\eta) v_\omega^2 + F_3(\eta) v_\omega^3 + F_4(\eta) v_\omega^4, \quad (5)$$

with

$$F_2(\eta) = -\frac{452}{87} - \frac{1139}{522}\eta, \quad (6a)$$

$$F_3(\eta) = \frac{309}{58} \pi, \quad (6b)$$

$$F_4(\eta) = -\frac{71345}{22968} + \frac{36761}{2088}\eta + \frac{147101}{68904}\eta^2. \quad (6c)$$

Finally, λ^i in Eq. (3) is a tangential unit vector directed in the same sense as the relative orbital velocity $v^i \equiv v_1^i - v_2^i$, v_1^i and v_2^i being the velocities of the masses m_1 and m_2 respectively. Note that the test-mass limit ($\eta \rightarrow 0$) of the function $F(v_\omega)$ has been first numerically evaluated in Ref. [16]. As we shall see below, one of the important differences between our treatment and the one of Ref. [5] will concern the continuation of the linear momentum flux Eq. (3) (derived for circular orbits above the LSO) to the (non circular) plunging orbit below the LSO.

In the next section, we present our prescription to compute the linear momentum flux and the related velocity of center of mass. Section III contains a summary of the ‘modified’ EOB approach that is used to describe the late stages of binary inspiral and plunge, followed by a detailed account of the numerical procedure that will result in the determination of the associated gravitational radiation driven recoil. We also present in that section analytical insights into our numerical estimates. In Sec. IV, we describe how we smoothly match the merger and the resultant ring down phases and the computation of the recoil of the final black hole. We present our results, conclusions and future directions in Sec. V.

³ We conventionally assume henceforth that $m_1 \geq m_2$ so that $\frac{m_1 - m_2}{M} = +\sqrt{1 - 4\eta}$.

II. QUASI-NEWTONIAN FORMULAS FOR LINEAR MOMENTUM FLUX AND RELATED RECOIL

In the EOB formalism, one finds that the relative orbital dynamics of a binary black hole system is most conveniently described in a “Schwarzschild-like” coordinate system, to which is associated an “effective metric” of the form

$$ds_{\text{eff}}^2 = -A(R) dT_{\text{eff}}^2 + \frac{D(R)}{A(R)} dR^2 + R^2 (d\theta^2 + \sin^2 \theta d\varphi^2) . \quad (7)$$

We shall work here to 2PN accuracy, in which case the “effective metric coefficients” $A(R)$ and $D(R)$ are given by

$$A(R) = 1 - \frac{2M}{R} + 2\eta \left(\frac{M}{R}\right)^3 , \quad (8a)$$

$$D(R) = 1 - 6\eta \left(\frac{M}{R}\right)^2 . \quad (8b)$$

It was shown in Ref. [7] that the complicated and badly convergent second post-Newtonian expanded dynamics of a binary system could be mapped onto the much simpler (and better convergent) dynamics of an auxiliary test particle falling along a geodesic of the effective metric, Eq. (7). Note that, even in the equal mass limit ($\eta = \frac{1}{4}$), the effective metric coefficients, given by Eqs. (8), differ only slightly from those of a Schwarzschild metric (i.e. $A_S(R) = 1 - \frac{2M}{R}$; $D_S(R) = 1$). As emphasized in Ref. [7] this property makes it useful to describe the EOB dynamics in the Schwarzschild-type coordinates of Eq. (7), rather than, say, in Arnowitt-Deser-Misner or harmonic coordinates which would lead either to a (badly convergent) infinite series of PN corrections, or to more complicated “resummed” expressions.

One of the important features of the present study will be to express the flux of linear momentum radiated away from a compact binary directly in terms of the quasi-Schwarzschild coordinates R and φ used in the effective one body metric, Eq. (7), and of their time-derivatives, notably the angular velocity $\Omega = \frac{d\varphi}{dT}$. Our work will often rely on the use of quantities having simple (and “quasi-Newtonian”) expressions in terms of quasi-Schwarzschild coordinates R and φ . Let us first motivate this use of quasi-Newtonian quantities expressed in quasi-Schwarzschild coordinates.

In the test-mass limit, it is a striking feature of Schwarzschild coordinates that they often allow one to convert Newtonian results into exact, or near-exact, Einsteinian results.

A famous example of that is the location (à la Mitchell-Laplace) of the Schwarzschild horizon which is correctly given by using the purely Newtonian energy conservation: $c(r)^2/2 - GM/R = c(\infty)^2$. In addition, the angular frequency along circular geodesics in a Schwarzschild background is described, in Schwarzschild coordinates, by the usual Kepler law: $GM = \Omega^2 R^3$, so that the linear velocity $v \equiv \Omega R$ is given by the usual Newtonian formula $v^2 = GM/R$. Here we shall use the remarkable fact that this closeness extends to gravitational radiation properties. In particular, the total energy flux emitted by circular geodesics into gravitational waves is numerically very well approximated by the simple quasi-Newtonian formula obtained by writing the leading-order quadrupole formula [$dE/dt \propto (d^3 I_{ij}/dt^3)^2 \propto \Omega^6 (I_{ij})^2$] in Schwarzschild coordinates. Indeed, this yields $dE/dt = \frac{32}{5} \eta^2 \Omega^6 R^2$ which is quite close to the complete general relativistic answer [34]: even at the LSO, $R_{\text{LSO}} = 6M$, the quasi-Newtonian result $\frac{32}{5} \eta^2 \Omega^6 R^2$ is only 12% smaller than the full Einsteinian one, and the agreement is better for orbits above the LSO. A look at Fig. 2 in Ref. [16] shows that a similar type of agreement holds also for the flux of linear momentum down to the LSO. Note that is crucial in this comparison to “interpret” quasi-Newtonian results in terms of Schwarzschild coordinates. For instance, if one were to insert harmonic coordinates R_h in the quadrupolar result $dE/dt = \frac{32}{5} \eta^2 \Omega^6 R_h^2$ (and uses a corresponding harmonic-coordinate Kepler law $M = \Omega^2 R_h^3$) one would obtain an estimate for the energy flux which would be larger than the correct one, at the LSO ($R_h = 5$), by a factor $\simeq 2.19$.

Regarding the plunging orbits below the LSO, another important feature of our treatment is that we do not wish to insert in the leading-order, “quasi-Newtonian”, energy and linear momentum fluxes the usually assumed “Kepler-type” law relating the angular velocity Ω to the radius R . Indeed, Kepler’s law (which reads $GM = \Omega^2 R^3$ in the test-mass limit $\eta \rightarrow 0$ and in Schwarzschild coordinates) is only valid, below the LSO, along the physically irrelevant sequence of unstable circular orbits corresponding to a *maximum* of the effective radial potential⁴. The “violation” of Kepler’s law during the plunge will be illustrated in Fig. 2 below.

With this motivation, let us derive from scratch the quasi-Newtonian result for the linear

⁴ Indeed, this maximum of the effective potential corresponds to an unphysical angular momentum $p_\varphi > p_\varphi^{\text{LSO}}$. In contrast, the physically relevant plunge motion corresponds to $p_\varphi < p_\varphi^{\text{LSO}}$ and thereby to a particle gliding down a flattish effective potential having no maximum (nor minimum) anymore, i.e, a potential near but below the lowest radial potential plotted in Fig. 1 of Ref. [7].

momentum flux. We start from the following leading order formula, available in Ref. [15],

$$\mathcal{F}_{\mathbf{P}}^x + i \mathcal{F}_{\mathbf{P}}^y = \frac{1}{336 \pi} \left\{ \sqrt{14} I^{(3)2-2} I^{(4)31} + \sqrt{210} I^{(3)22} I^{(4)3-3} - 14 i I^{(3)2-2} S^{(3)21} \right\}, \quad (9)$$

where $\mathcal{F}_{\mathbf{P}}^x$ and $\mathcal{F}_{\mathbf{P}}^y$ are the x and y components of the linear momentum flux. Here I^{lm} and S^{lm} denote the ‘‘mass’’ and ‘‘spin’’ (or ‘‘current’’) radiative multipole moments of the binary, while $I^{(3)lm}$ denotes the third time derivative of I^{lm} . Under complex conjugation I^{lm} and S^{lm} transform as

$$I^{lm*} = (-1)^m I^{l-m}, \quad S^{lm*} = (-1)^m S^{l-m}. \quad (10)$$

We display below the relevant I^{lm} and S^{lm} required to compute the leading order contribution to $\mathcal{F}_{\mathbf{P}}^x + \mathcal{F}_{\mathbf{P}}^y$ for compact binaries in circular orbits, taken from Ref. [35],

$$\frac{I^{22}}{M} = \frac{2}{5} \sqrt{10 \pi} \eta R^2 e^{-2i\varphi}, \quad \frac{S^{21}}{M} = -\frac{8}{15} \sqrt{10 \pi} \eta \sqrt{1-4\eta} R^3 \Omega e^{-i\varphi}, \quad (11a)$$

$$\frac{I^{31}}{M} = -\frac{2}{105} \sqrt{35 \pi} \eta \sqrt{1-4\eta} R^3 e^{-i\varphi}, \quad \frac{I^{33}}{M} = \frac{2}{63} \sqrt{21 \pi} \eta \sqrt{1-4\eta} R^3 e^{-3i\varphi}, \quad (11b)$$

where $\Omega = \frac{d\varphi}{dT}$. The exact expression for, say, $I^{22} \propto \frac{d^3(R^2 e^{-2i\varphi})}{dT^3}$ contains several terms proportional to $\frac{d^3\varphi}{dT^3}$, $\frac{dR}{dT} \frac{d^2\varphi}{dT^2}$, $\dots \frac{d^3R}{dT^3}$. In the following, we consider an inspiralling and plunging relative orbit. For such an orbit, the derivatives $\frac{d^n R}{dT^n}$ do not vanish. However, as already mentioned above, it was pointed out in Ref. [8] that even during the ‘‘plunge’’ following the LSO crossing, the radial motion, characterized by $\frac{dR}{dT}$, remained small compared to the azimuthal one $R \frac{d\varphi}{dT}$. We shall take advantage of this fact to simplify the expression of the time-differentiated multipole moments entering Eq. (9) by keeping only the terms proportional to the time-derivatives of the azimuthal angle φ . We neglect also $\frac{d^2\varphi}{dT^2} = \frac{d\Omega}{dT}$ compared to $\frac{d\varphi}{dT} = \Omega$. This yields the simplified expression

$$(\mathcal{F}_{\mathbf{P}}^x + i \mathcal{F}_{\mathbf{P}}^y)^{\text{leading order}} = -i \frac{464}{105} f(\eta) R^5 \Omega^7 e^{i\varphi}. \quad (12)$$

An important difference between expression (12) and the earlier quoted expressions for linear momentum fluxes, namely, Eqs. (2) and (3), is that the proportionality to $R^5 \Omega^7$ was directly obtained from the original flux formula, Eq. (9), *without explicitly using* any ‘‘Kepler-like equation’’ linking R to Ω . We shall see later that this difference significantly affects the estimate of the final recoil velocity associated to the linear momentum flux (12).

In order to obtain the velocity of the center of mass, we then invoke linear momentum balance, namely,

$$M \frac{d}{dT} (v_{\text{com}}^x + i v_{\text{com}}^y) = -(\mathcal{F}_{\mathbf{P}}^x + i \mathcal{F}_{\mathbf{P}}^y), \quad (13)$$

where v_{com}^x and v_{com}^y are the x and y components of the center of mass velocity vector \mathbf{v}_{com} .

At this stage, it is convenient to introduce rescaled, dimensionless radial, time and frequency variables, namely, $r = \frac{R}{M}$, $t = \frac{T}{M}$, and $\omega = \frac{d\varphi}{dt} = M\Omega$. This leads to the following differential equation for $v_{\text{com}}^x + i v_{\text{com}}^y$

$$\frac{d}{dt} (v_{\text{com}}^x + i v_{\text{com}}^y) = i \frac{464}{105} f(\eta) r^5 \omega^7 e^{i\varphi}. \quad (14)$$

This leading order ‘‘quasi-Newtonian’’ result will be the basis of our investigation. We shall also discuss below how to use the 2PN correction terms derived in Ref. [5] [see Eq. (3)] to improve the accuracy of Eq. (14).

In this paper, in order to obtain an estimate for the velocity of the center of mass during the late inspiral and subsequent plunge phases, we shall numerically integrate Eq. (14) along with the differential equations that define the EOB dynamics.

In the next section, we summarize the EOB dynamics applicable to non-spinning compact binaries of arbitrary mass ratio moving in quasi-circular orbits during the inspiral phase [8]. We also describe, in some detail, how we solve the relevant set of differential equations to obtain an EOB based estimate for the recoil during the late inspiral and the subsequent plunge phases. We shall also complement our numerical estimates by analytic arguments allowing one to understand in simple terms the main characteristics, and the order of magnitude, of our results.

III. THE LATE INSPIRAL, PLUNGE PHASES AND THE ASSOCIATED RECOIL USING THE EOB APPROACH

Let us first summarize the EOB approach relevant for describing the inspiral and plunge phases of a compact binary. At the 2PN accuracy, the mapping between the full two-body 2PN dynamics, and the much simpler geodesic dynamics in the EOB metric, given by Eq. (7), leads to an EOB dynamics described by the following Hamiltonian (expressed in the scaled variables $r \equiv \frac{R}{M}$, $t = \frac{T}{M}$, $\omega = \frac{d\varphi}{dt} = M\Omega$, and in polar coordinates)

$$\mathcal{H}(r, p_r, p_\varphi) = \frac{1}{\eta} \sqrt{1 + 2\eta \left[\sqrt{A(r) \left(1 + \frac{p_r^2}{B(r)} + \frac{p_\varphi^2}{r^2} \right)} - 1 \right]}, \quad (15)$$

where $A(r)$ and $B(r)$ [see Eqs. (7), and (8) above] are given by

$$A(r) = 1 - \frac{2}{r} + \frac{2\eta}{r^3}, \quad (16a)$$

$$B(r) = \frac{D(r)}{A(r)} = \frac{1}{A(r)} \left(1 - \frac{6\eta}{r^2} \right). \quad (16b)$$

More precisely, the explicit form of the EOB equations of motion read

$$\frac{dr}{dt} = \frac{\partial \mathcal{H}(r, p_r, p_\varphi)}{\partial p_r}, \quad (17a)$$

$$\frac{d\varphi}{dt} \equiv \omega = \frac{\partial \mathcal{H}(r, p_r, p_\varphi)}{\partial p_\varphi}, \quad (17b)$$

$$\frac{dp_r}{dt} = -\frac{\partial \mathcal{H}(r, p_r, p_\varphi)}{\partial r}, \quad (17c)$$

$$\frac{dp_\varphi}{dt} = \mathcal{F}_\varphi. \quad (17d)$$

The right-hand side of the last equation expresses the loss of angular momentum under gravitational radiation reaction. Its explicit form will be discussed below.

As mentioned earlier, to obtain an estimate for the recoil during the late inspiral and subsequent plunge, we solve along with the above set of differential equations, the one for $v_{\text{com}}^x + i v_{\text{com}}^y$, given by Eq. (14), namely,

$$\frac{d}{dt} (v_{\text{com}}^x + i v_{\text{com}}^y) = i \frac{464}{105} f(\eta) r^5 \omega^7 e^{i\varphi} \tilde{F}. \quad (18)$$

Here the supplementary factor $\tilde{F} = 1 + \mathcal{O}(v^2) + \mathcal{O}(v^3) + \mathcal{O}(v^4)$, resulting from Ref. [5], is added to improve the accuracy of the leading-order, quasi-Newtonian result, given by Eq. (2), to the 2PN level. Its explicit form along our quasi-circular, sub LSO, orbits is discussed in the following subsection.

A. Inclusion of 2PN corrections in the fluxes of linear and angular momenta

In this subsection, we describe the construction of 2PN accurate expressions for the recoil (linear momentum flux) factor \tilde{F} in Eq. (18), as well as for the radiation reaction force \mathcal{F}_φ (the angular momentum flux), appearing in Eq. (17d).

Let us start by discussing the value of the correcting factor \tilde{F} (and of its analog in the energy flux) during the adiabatic inspiral phase. During this phase, our construction is facilitated by the fact that the orbital dynamics closely follows the *one parameter sequence of stable circular orbits* that exists above the LSO. In the EOB formalism, these orbits represent the *minima*, with respect to r , of the Hamiltonian $\mathcal{H}_{\text{circ}}(r, p_\varphi) \equiv \mathcal{H}(r, p_r = 0, p_\varphi)$.

Equivalently, we see from Eq. (15) that they are obtained by minimizing with respect to r the effective potential

$$w(r, p_\varphi) = A(r) \left(1 + \frac{p_\varphi^2}{r^2} \right), \quad (19)$$

with $A(r)$ given by Eq. (16a). Minimizing $w(r, p_\varphi)$ with respect to r yields the following relation linking r to p_φ^2 [see Eqs. (4.5) and (4.6) of Ref. [8]]

$$p_\varphi^2|_{\text{circ}} = r \frac{1 - \frac{3\eta}{r^2}}{1 - \frac{3}{r^2} + \frac{5\eta}{r^3}}. \quad (20)$$

Inserting the latter result in the definition of the angular velocity, namely $\omega \equiv \frac{\partial \mathcal{H}(r, p_r, p_\varphi)}{\partial p_\varphi}$, also considered along circular orbits [i.e., $\omega_{\text{circ}} \equiv \frac{\partial \mathcal{H}_{\text{circ}}(r, p_\varphi)}{\partial p_\varphi}$], then yields a relation connecting ω_{circ} to r . This 2PN generalization of Kepler's third law reads [see Eqs. (4.8) of Ref. [8]]

$$\omega_{\text{circ}}^2 = \frac{1}{r^3} \left(\frac{1 - \frac{3\eta}{r^2}}{1 + 2\eta(\sqrt{w} - 1)} \right). \quad (21)$$

In the test mass limit, $\eta \rightarrow 0$, we recover the well-known fact that circular orbits in a Schwarzschild geometry (in Schwarzschild coordinates) satisfy the standard Kepler law: $\omega^2 r^3 = 1$. It is then traditional to use as PN order parameter $v_\omega \equiv \omega^{1/3} = \mathcal{O}(v/c)$, or equivalently $x_\omega \equiv v_\omega^2 \equiv \omega^{2/3} = \mathcal{O}(v^2/c^2)$, to describe all possible PN corrections, be they proportional to the square of the linear azimuthal velocity $v_\varphi \equiv \omega r$, or to the gravitational potential $u \equiv \frac{1}{r}$. Indeed, when $\eta = 0$, we have the simple, Kepler-like links: $(\omega r)^2 = \frac{1}{r} = v_\omega^2 = \omega^{2/3}$. To extend these simple links to the comparable mass case $\eta \neq 0$ (and to the sub-LSO quasi-circular orbits), let us introduce the function

$$\psi(r, p_\varphi) \equiv \frac{1 + 2\eta \left(\sqrt{w(r, p_\varphi)} - 1 \right)}{1 - \frac{3\eta}{r^2}}, \quad (22)$$

and the definition

$$r_\omega \equiv r \left(\psi(r, p_\varphi) \right)^{1/3}. \quad (23)$$

These definitions are such that, along circular orbits, we can still write a simple Kepler-looking law

$$\omega^2 r_\omega^3 = 1, \quad (24)$$

as well as its usual consequences, such as $(\omega r_\omega)^2 = \frac{1}{r_\omega} = \omega^{2/3} \equiv v_\omega^2$. We can then use these relations to rewrite any 2PN-accurate result expressed (along circular orbits) in terms of $v_\omega \equiv \omega^{1/3}$ in terms of ω, r and ψ .

For instance, the 2PN accurate linear momentum flux [5], Eq. (3), is proportional to $v_\omega^{11} F(v_\omega) = \omega^7 r_\omega^5 F(\omega r_\omega) = \omega^7 (r \psi^{1/3})^5 F(\omega r \psi^{1/3})$. Our approach leads us to considering that the basic “quasi-Newtonian” expression for the linear momentum flux is proportional to $\omega^7 r^5$ [see Eq. (12) above]. In other words, we are naturally led to writing the 2PN-accurate flux in the form of Eq. (18) with a 2PN-correction factor \tilde{F} given by

$$\tilde{F}(r, p_\varphi) = \left(\psi(r, p_\varphi) \right)^{5/3} F(\omega r \psi^{1/3}). \quad (25)$$

Let us first note that for circular orbits *above the LSO* (for which all the above reasonings are fully justified) the “correcting factors” linked to the function ψ are very close to 1. More precisely, if we consider the case $\eta = 0.2$ (which is the most important one) ψ tends to 1 when $r \rightarrow \infty$, and as r decreases ψ first decreases to reach a minimum $\psi_{\min} \simeq 0.9882$ around $r \simeq 9.2$. Afterwards, it increases to reach $\psi_{\text{LSO}} \simeq 0.9921$ when $r = r_{\text{LSO}} \simeq 5.8$. Note that the factor $\psi_{\text{LSO}}^{1/3} \simeq 0.9974$ modifying the azimuthal velocity $v_\varphi = \omega r$ in Eq. (25) differs only by $\sim 3 \times 10^{-3}$ from *unity*. As for the total 2PN correcting factor \tilde{F} , one can see that it represents, above the LSO, a relatively modest modification of the quasi-Newtonian momentum flux. If we evaluate it by inserting the straightforward 2PN-expanded version of the function F , Eq. (5), into Eq. (25), we find a result of order 1.24 at the LSO.

Note also that, in the EOB approach, it is natural to consider as basic PN-ordering parameter the azimuthal velocity,

$$v_\varphi = \omega r, \quad (26)$$

which is an *invariantly defined* quantity⁵.

Up to this stage we have been assuming that we were considering quasi-circular orbits corresponding to a local minimum of the effective radial potential. This happens when one is above the LSO. In contrast, when considering the continuation of the orbit below the LSO, the circular orbits [and their consequences, such as Eq. (21)] are no longer physically relevant because they correspond to unstable maxima of $w(r, p_\varphi)$, given by Eq. (19). When considering quasi-circular orbits *below the LSO*, one should, in principle, re-derive from scratch the 2PN-accurate linear momentum flux, *without assuming* any Kepler-like law of type Eq. (21) or Eq. (24). The 2PN corrections then become functions of three independent

⁵ Indeed, in the EOB formalism, both ω and the effective-metric Schwarzschild radius r are invariant quantities.

variables: r, p_φ , and p_r , or equivalently, r, ω , and p_r . As pointed out in Refs. [7, 8] the motion remains “quasi-circular” during the plunge in the sense that the contributions linked to p_r^2 stay numerically small compared to those linked to p_φ^2 , allowing one to neglect p_r^2 . The 2PN corrections during the plunge then become functions of two independent variables, namely, r and p_φ . In view of the arguments recalled above pointing to a remarkable closeness between exact Einsteinian results and quasi-Newtonian results expressed in terms of Schwarzschild-type coordinates, we consider it likely that the momentum flux during the plunge follows more or less the quasi-Newtonian behavior $\mathcal{F} \propto r^5 \omega^7$. To ensure continuity with the 2PN-correcting factor Eq. (25), which is present above the LSO, we shall assume here that 2PN corrections below the LSO are sufficiently well estimated by continuing to use the expression (25)⁶.

Note that this assumption differs from the one made in Refs. [8] and [5] which consisted in continuing to use the expressions giving the 2PN corrections as functions of $v_\omega \equiv \omega^{1/3}$. Within the spirit of the EOB formalism, we feel that it is not very plausible to continue to use v_ω as basic PN ordering parameter, and to express quantities only in terms of it. Indeed, the definition of v_ω makes sense only so far as a Kepler-like law relating ω to r continues to hold. This is no longer the case below the LSO (as will be illustrated in Fig. 2 below). In absence of such a Kepler law, we prefer to remain close to what is suggested by the leading-order quasi-Newtonian result $\mathcal{F} \propto r^5 \omega^7$. We shall further discuss below the importance of this choice.

Let us apply the same philosophy to the estimate of the radiation reaction term \mathcal{F}_φ , appearing in Eq. (17d), below the LSO. It was shown in Refs. [36] and [8] that a good estimate for \mathcal{F}_φ *above the LSO* is given by

$$\mathcal{F}_\varphi^{\text{circ}} = -\frac{32}{5} \eta v_\omega^7 \frac{\hat{f}_{\text{DIS}}(v_\omega; \eta)}{1 - \frac{v_\omega}{v_{\text{pole}}}}, \quad (27)$$

where \hat{f}_{DIS} is a 2.5PN (v^5 -accurate) Padé approximant for the angular momentum flux. It is defined, *e.g.* in Eqs. (3.28)-(3.36) of Ref. [8] [Note, however that the 2.5PN coefficient

⁶ Note, however, that we no longer assume the link, provided by Eq. (20). Indeed, this link exhibits an infinite growth of p_φ as r tends to the (η -modified) “light-ring”, where $r^3 - 3r^2 + 5\eta = 0$. As we know instead that p_φ stays below its LSO value during the plunge (and evolves much more slowly than r), it seems a priori better to express the PN corrections only in terms of well behaved quantities, such as r, ω , and p_φ .

there must be corrected to a new value due to Ref. [37].]. The definition of \hat{f}_{DIS} depends on the choice for the location of the “pole” v_{pole} . Following Ref. [36] [and also Ref. [8]], we use the value of v_{pole} defined in Eq. (3.37) of Ref. [8]. [As shown in Ref. [38] the precise choice of v_{pole} is not very important and, for instance, the value $v_{\text{pole}} = v_{\text{pole}}^{\eta=0} = \frac{1}{\sqrt{3}}$ would suffice.] Ref. [8] proposed to continue using Eq. (27), expressed in terms of $v_{\omega} \equiv \omega^{1/3}$, even below the LSO. Here, consistently with the arguments presented above, we shall instead use a different continuation for \mathcal{F}_{φ} below the LSO. To derive it we need to know what is the analog, for the angular momentum loss, for the “quasi-Newtonian” result, displayed in Eq. (9). Consistently with what was briefly mentioned above about the energy flux, we know [see, e.g., Eq. (4.23) of Ref. [15]] that the leading term in the angular momentum loss $\frac{dJ_z}{dt}$ is $\propto I^{2-2} \times I^{22}$. Remembering the leading-order expression for the quadrupole moment I^{22} , given in Eqs. (11), we see that the “quasi-Newtonian” expression for \mathcal{F}_{φ} is $\propto \frac{d^2(R^2 e^{2i\varphi})}{dT^2} \times \frac{d^3(R^2 e^{-2i\varphi})}{dT^3}$ and therefore (in the quasi-circular approximation $\dot{r} \ll r\dot{\varphi}$) $\propto r^4 \omega^5$. This shows that one should rewrite the leading factor v_{ω}^7 in Eq. (27) as $\frac{v_{\omega}^5}{r_{\omega}}$, i.e., $\frac{(\omega r_{\omega})^5}{r_{\omega}} = \omega^5 r_{\omega}^4$. In other words, this leads us to using, below the LSO, the following expression for the radiation reaction force \mathcal{F}_{φ} in Eq. (27),

$$\mathcal{F}_{\varphi}(r, p_{\varphi}, p_r) = -\frac{32}{5} \eta \omega^5 (r \psi^{1/3})^4 \frac{\hat{f}_{\text{DIS}}(\omega r \psi^{1/3}; \eta)}{1 - \frac{\omega r \psi^{1/3}}{v_{\text{pole}}}}, \quad (28)$$

where the factor ψ is a function of r and p_{φ} , defined in Eq. (22) and where $\omega = \omega(r, p_r, p_{\varphi})$ is defined by the second equation in Eqs. (17).

Let us finally discuss the question of the re-summation of the 2PN-accurate correction factor, Eq. (25). When comparing the straightforward, PN-expanded versions of the 2PN factor $F(v_{\omega})$, given by Eq. (5) and derived in Ref. [5], entering the 2PN accurate linear momentum flux to its analog in the energy (or angular momentum) flux, namely,

$$F_{\text{E}}(v_{\omega}) = \text{Taylor} \left[\frac{\hat{f}_{\text{DIS}}(v_{\omega})}{1 - \frac{v_{\omega}}{v_{\text{pole}}}} \right] = 1 + F_{\text{E}2}(\eta) v_{\omega}^2 + F_{\text{E}3}(\eta) v_{\omega}^3 + F_{\text{E}4}(\eta) v_{\omega}^4 + \dots, \quad (29)$$

where $F_{\text{E}2} = -\left(\frac{1247}{336} + \frac{35}{12} \eta\right)$, $F_{\text{E}3} = 4\pi$, and $F_{\text{E}4} = \left(-\frac{44711}{9072} + \frac{9271}{504} \eta + \frac{65}{18} \eta^2\right)$ [see Ref. [39]], one notices that these two “Taylor expansions”, i.e., expressions for $F(v_{\omega})$ and $F_{\text{E}}(v_{\omega})$, are rather similar. The corresponding Taylor coefficients F_n [in $\mathcal{F}_{\mathbf{P}}^{i(\text{BQW})}$] and $F_{\text{E}n}$ [in \mathcal{F}_{E} or \mathcal{F}_{φ}] have the same signs, similar sensitivities to the value of η , and roughly similar magnitudes. Indeed, we can roughly consider that $F_n \sim 1.3 F_{\text{E}n}$. In addition, the same argument which

was used in Ref. [36] to show that the “exact” function $F_E(v)$ (analytically continued from its behavior above the LSO) has, in the limit $\eta \rightarrow 0$, a pole at $v_{\text{pole}}^{\eta=0} = \frac{1}{\sqrt{3}}$ (i.e. at the light ring) can be applied to the function $F(v)$, appearing in Eq. (3) for $\mathcal{F}_{\mathbf{P}}^{i(\text{BQW})}$, to conclude that $F(v)$ also has, when $\eta \rightarrow 0$, a pole at the same (light-ring value) $v_{\text{pole}}^{\eta=0} = \frac{1}{\sqrt{3}}$. This suggests that a Padé re-summation of the $F(v)$, given by Eq. (5), might improve the convergence behavior of $F(v)$, which is currently known only up to 2PN accuracy. On the other hand, the similarity between the two Taylor expansions F_n and F_{E_n} (i.e. the fact that $F_n \sim 1.3 F_{E_n}$) suggests that both the successive Taylor and Padé approximants of $F(v)$ will have convergence properties similar to the corresponding approximants of F_E . By looking at the convergence properties⁷ (when $\eta \rightarrow 0$) of the Taylor or Padé approximants of F_E , as displayed in Fig. 3 of Ref. [36], we observe that, among the approximants of PN order v^n with $n \leq 5$, the best one is the v^5 -accurate (2.5PN level) Padé approximant [i.e the one used in Eq. (27) above]. However, the 2.5PN coefficient, $F_5(\eta)$, is not currently known for the analogous linear-momentum flux $\mathcal{F}_{\mathbf{P}}^{i(\text{BQW})}$. From Fig. 3 in Ref. [36], we expect the v^4 -accurate Taylor approximant of $F(v)$ to overestimate $F^{\text{exact}}(v)$ when $v \leq 0.4$ and to underestimate it when $v \geq 0.4$ (note that $v_{\omega}^{\text{LSO}}(\eta = 0.2) \simeq 0.414$). On the other hand, we expect the v^4 -accurate Padé approximant to follow $F^{\text{exact}}(v)$ better, but to underestimate it for all values of v . In the absence of knowledge about the 2.5PN contributions $F_5(\eta)$, we shall compare here the results obtained both from using the v^4 -accurate Taylor approximant, given by Eq. (5), and its corresponding Padé approximant, of the form

$$F_{\mathbf{P}}(v) = \frac{\hat{g}(v)}{1 - \frac{v}{v_{\text{pole}}}}, \quad (30)$$

where we take, for simplicity, $v_{\text{pole}} = \frac{1}{\sqrt{3}}$, and with

$$\hat{g}(v) = \frac{1}{1 + \frac{c_1 v}{1 + \frac{c_2 v}{1 + \frac{c_3 v}{1 + c_4 v}}}}. \quad (31)$$

⁷ Note that the argument used in Ref. [5] (namely: the closeness of the v^3 - and v^4 -accurate Taylor approximants suggests that a good convergence is reached with 2PN accuracy) is not conclusive in view of what happens for the similar Taylor expansion of $F_E(v)$. Indeed, one can easily check (say, when $\eta = 0$ or $\eta = 0.2$) that the v^3 and v^4 accurate Taylor approximants of $F_E(v)$ are close to each other, while the next v^5 -accurate, Taylor approximant of $F_E(v)$ is quite far away from both of them (and also from the exact result, when $\eta \rightarrow 0$). This is linked to the fact, emphasized in Ref. [36], that Taylor approximants have rather erratic convergence properties as the PN order increases (while, by contrast, the Padé approximants have a more monotonic convergence, though they tend to accumulate somewhat below the exact result).

Note that $\hat{g}(v)$ is constructed quite similarly to $\hat{f}_{\text{DIS}}(v)$, i.e. by applying Eqs. (3.29),(3.31),(3.34) and (3.35) of Ref. [8], while replacing Eqs. (3.32) and (3.33) in Ref. [8] by the coefficients F_2, F_3 , and F_4 entering Eq. (5) above.

B. Initial conditions for the dynamics

Before we present our numerical results, let us explain how we prescribe initial conditions when solving these differential equations. The initial conditions for r and φ are arbitrary and prescribe the initial radial separation of the binary in the center of mass frame and its associated angular position. The initial values for p_r and p_φ are obtained with the help of the adiabatic approximation to the EOB inspiral, introduced in Sec. IV (A) of Ref. [8]. This approximation is obtained by imposing $p_r = 0$ in the EOB dynamics, which implies that the effective body follows an adiabatic sequence of circular orbits with decreasing energy due to the emission of gravitational radiation. This zeroth-order adiabatic approximation (which turns out to be enough for our purpose) provides the following expressions for p_φ and ω

$$p_\varphi|_{\text{adiab}} = \left(\frac{r^2 (r^2 - 3\eta)}{r^3 - 3r^2 + 5\eta} \right)^{1/2}, \quad (32a)$$

$$\omega|_{\text{adiab}} = \left(\frac{(1 - \frac{3\eta}{r^2})}{r^3 (1 + 2\eta [\sqrt{z(r)} - 1])} \right)^{1/2}, \quad (32b)$$

where $z(r) = \frac{r^3 A^2(r)}{r^3 - 3r^2 + 5\eta}$ with $A(r)$ given by Eq. (16a).

The initial value for $v_{\text{com}}^x + i v_{\text{com}}^y$ is obtained by using

$$v_{\text{com}}^x|_{\text{initial}} = \frac{464}{105} \eta^2 \sqrt{1 - 4\eta} \frac{\cos \varphi}{r^4}, \quad v_{\text{com}}^y|_{\text{initial}} = \frac{464}{105} \eta^2 \sqrt{1 - 4\eta} \frac{\sin \varphi}{r^4}, \quad (33)$$

derivable from Eqs. (2). In the next subsection, we present analytical insights into the physical behavior underlying our numerical estimates.

C. Linear momentum loss during inspiral and plunge

Before numerically implementing our strategy for estimating the recoil during the late inspiral, the subsequent plunge and the final merger, let us outline the main physical features of our calculation⁸. Let us first note that the final recoil velocity is essentially given by an

⁸ See below for the effects of ring-down.

integral of the form

$$(v_{\text{com}}^x + i v_{\text{com}}^y)^{\text{terminal}} = i \mathcal{I} \equiv i \int_{-\infty}^{+\infty} dt a(t) e^{i\varphi(t)}, \quad (34)$$

where $\varphi(t)$ is the orbital phase, while the ‘‘amplitude’’ $a(t) = |\mathcal{F}_{\mathbf{P}}|$ is proportional to $r^5 \omega^7 \tilde{F}$. The first important point to realize is that the value of the above integral \mathcal{I} is dominated by what happens in the time intervals where the amplitude $a(t)$ varies in a ‘‘non-adiabatic’’ manner. Indeed, let us first assume that the amplitude $a(t)$ always varies in an adiabatic manner with respect to the orbital phase $\varphi(t)$, i.e. let $\frac{\dot{a}}{a} \ll \dot{\varphi}$. This can be conveniently formalized by replacing the phase factor $e^{i\varphi}$ by $e^{i\varphi/\epsilon}$, where ϵ is a formal ‘‘small parameter’’ measuring how small the ratio $\frac{\dot{a}}{a}/\frac{\dot{\varphi}}{\epsilon} \sim \mathcal{O}(\epsilon)$ is. Using the fact that $\varphi(t)$ is a monotonic function of time, one can use φ , instead of t , in the above integral. After replacing $a(t)$ by $\mathcal{A}(\varphi) \equiv \frac{a(t)}{\dot{\varphi}(t)}$, we get $\mathcal{I}(\epsilon) = \int_{-\infty}^{+\infty} d\varphi \mathcal{A}(\varphi) e^{i\varphi/\epsilon}$. Using $e^{i\varphi/\epsilon} = \frac{\epsilon}{i} \left(\frac{d e^{i\varphi/\epsilon}}{d\varphi} \right)$ and integrating by parts, we find $\mathcal{I}(\epsilon) = i\epsilon \int d\varphi \mathcal{A}'(\varphi) e^{i\varphi/\epsilon}$, where we employed the vanishing of $\mathcal{A}(\varphi)$ at $\pm\infty$ (see below). Repeating this procedure, we get

$$\mathcal{I}(\epsilon) = (i\epsilon)^n \int_{-\infty}^{+\infty} d\varphi \mathcal{A}^{(n)}(\varphi) e^{i\varphi/\epsilon}, \quad (35)$$

where $\mathcal{A}^{(n)}(\varphi)$ is the n -th derivative of \mathcal{A} w.r.t φ . This (well-known) result means that, when $\epsilon \rightarrow 0$, $\mathcal{I}(\epsilon) = \mathcal{O}(\epsilon^n)$ for any integer n . In other words, $\mathcal{I}(\epsilon)$ *vanishes faster than any power of ϵ* , if $a(t)$ varies adiabatically during the whole process. In most cases, this means that $\mathcal{I}(\epsilon)$ is exponentially small $\sim e^{-C/\epsilon^2}$, and therefore numerically negligible compared to the naive estimates of the type $\mathcal{I} \sim a_{\text{max}} \Delta t$, where Δt is a characteristic variation time, say $\Delta t \sim \frac{1}{\omega}$ with $\omega = \dot{\varphi}$, that one might have been tempted to make.

This mathematical reminder shows that the actual magnitude of the momentum flux $|\mathcal{F}_{\mathbf{P}}| = a(t)$ during the inspiral and the plunge is secondary with respect to the question of knowing the characteristic time-scale on which $|\mathcal{F}_{\mathbf{P}}|$ varies during the plunge. If $\frac{\dot{a}}{a}$ stayed always small compared to the orbital frequency $\omega = \dot{\varphi}$, the recoil would be a non-perturbative effect; and it would be practically hopeless to try to estimate it by starting from approximate analytical expressions. [On the other hand, we would know that the recoil is exponentially small, so that it would be astrophysically negligible.] However, the study of the time evolution of the amplitude $a(t)$ during the EOB plunge shows that, while it remains adiabatic ($\frac{\dot{a}}{a} \ll \dot{\varphi}$) during most of the inspiral and plunge, it becomes barely non-adiabatic near the moment where $a(t)$ reaches a *maximum* [at which point, the criterion for non-adiabaticity

must involve the *second* time derivative of $a(t)$]. This is illustrated in Fig. 2, which shows the evolution of the magnitude of the momentum flux, $|\mathcal{F}_{\mathbf{P}}|$, during the late inspiral and the plunge. This figure makes it clear that the characteristic evolution time scale for $a(t)$ is shortest near its maximum, i.e. for a (scaled) radius $r_{\max} \simeq 3.5$. Before discussing the consequences of this fact, let us outline how one can analytically understand why $|\mathcal{F}_{\mathbf{P}}|$ has the behavior exhibited in Fig. 2.

The main factor determining the behavior of $|\mathcal{F}_{\mathbf{P}}|$ is the product $r^5 \omega^7$ in Eq. (14). During the plunge, the evolution of r and ω are governed by the EOB equations of motion, namely Eqs. (17). In these equations, the radiative damping “force” \mathcal{F}_φ is crucial to drive the slow inspiral and to trigger the plunge, but was found to play a minor role once the plunge is well on its way [8, 40]. As a consequence, the evolution of ω during the plunge is approximately given by $\omega = \frac{\partial \mathcal{H}(r, p_r, p_\varphi)}{\partial p_\varphi}$, with $p_\varphi \simeq \text{constant}$ as well as $\mathcal{H} \simeq \text{constant}$ (zero-damping approximation). In this approximation, one thereby finds that ω is approximately proportional to the ratio $\frac{A(r)}{r^2}$ so that we can write, during the plunge, the approximate link

$$\omega_{\text{plunge}}(r) \approx \omega_{\text{LSO}} \frac{r_{\text{LSO}}^2}{A(r_{\text{LSO}})} \frac{A(r)}{r^2}. \quad (36)$$

The change in behavior of $\omega(r)$ between the inspiral (where Kepler’s third law $\omega^2 r^3 \approx \text{constant}$ holds approximately), and the plunge [where Eq. (36) holds instead] is illustrated in Fig. 3.

As a consequence of Eq. (36), we find that the behavior of the linear momentum flux during the plunge is approximately given by

$$|\mathcal{F}_{\mathbf{P}}| \propto r^5 \omega^7 \propto \frac{1}{r^9} \left(1 - \frac{2}{r} + \frac{2\eta}{r^3} \right)^7. \quad (37)$$

Denoting $u = \frac{1}{r}$, it is easily seen that $|\mathcal{F}_{\mathbf{P}}| \propto u^9 (1 - 2u + 2\eta u^3)^7$ reaches a maximum value when $(9 - 32u_{\max} + 60\eta u_{\max}^3) = 0$. When $\eta = 0.2$ (which corresponds to the maximum of the overall factor $f(\eta)$, given by Eq. (1), and thereby approximately to the maximum recoil), this gives $u_{\max} \simeq 0.29044$, corresponding to $r_{\max}^{\text{analytic}} = \frac{1}{u_{\max}} \simeq 3.4431$. This analytical argument agrees well with our numerical results. Indeed, we find that $|\mathcal{F}_{\mathbf{P}}|$, computed using the quasi-Newtonian version of Eq. (18), has a maximum around $r_{\max}^{\text{numerical}} \simeq 3.501$. One can even go further and analytically study the behavior of $|\mathcal{F}_{\mathbf{P}}|$ near its maximum. The most

important time scale there is defined by the curvature of $|\mathcal{F}_{\mathbf{P}}|$ near its maximum:

$$\tau_{\max}^2 \equiv -\frac{\mathcal{F}_{\mathbf{P}}^{\max}}{\left(\frac{d^2\mathcal{F}_{\mathbf{P}}}{dt^2}\right)_{\max}}, \quad (38)$$

where, for notational simplicity, we henceforth denote by $\mathcal{F}_{\mathbf{P}}$ the *modulus* of the momentum flux.

An important dimensionless quantity associated to the time scale τ_{\max} is the “quality factor” $Q \equiv \omega_{\max} \tau_{\max}$ associated to the “resonance peak” of $\mathcal{F}_{\mathbf{P}}$. Indeed, values of Q of order unity mean (as we shall find) that the evolution of $\mathcal{F}_{\mathbf{P}}$ near its maximum is just fast enough to be non-adiabatic there.

In view of the discussion above, this means that the recoil, i.e. (modulo a factor i) the integral \mathcal{I} , given by Eq. (34), will be dominated by what happens near the maximum of $\mathcal{F}_{\mathbf{P}}$. Therefore, we can analytically estimate \mathcal{I} by replacing $a(t) = \mathcal{F}_{\mathbf{P}} (\equiv |\mathcal{F}_{\mathbf{P}}|)$ by the local approximation (with $\bar{t} \equiv t - t_{\max}$)

$$a(t) \simeq \mathcal{F}_{\mathbf{P}}^{\max} + \frac{1}{2} \left(\frac{d^2\mathcal{F}_{\mathbf{P}}}{dt^2} \right)_{\max} \bar{t}^2 = \mathcal{F}_{\mathbf{P}}^{\max} \left(1 - \frac{1}{2} \frac{\bar{t}^2}{\tau_{\max}^2} \right) \simeq \mathcal{F}_{\mathbf{P}}^{\max} e^{-\frac{\bar{t}^2}{2\tau_{\max}^2}}, \quad (39)$$

and the phase $\varphi(t)$ by

$$\varphi(t) \simeq \varphi_{\max} + \dot{\varphi}_{\max} \bar{t} + \frac{1}{2} \ddot{\varphi}_{\max} \bar{t}^2 = \varphi_{\max} + \omega_{\max} \bar{t} + \frac{1}{2} \dot{\omega}_{\max} \bar{t}^2. \quad (40)$$

If we then consider the recoil acquired up to some given time \bar{t}' , its is given by a truncated Gaussian integral

$$(v_{\text{com}}^x + i v_{\text{com}}^y)(\bar{t}') \simeq i \mathcal{F}_{\mathbf{P}}^{\max} e^{i\varphi_{\max}} \int_{-\infty}^{\bar{t}'} d\bar{t} e^{-\frac{1}{2}\alpha\bar{t}^2 + \beta\bar{t}}, \quad (41)$$

where (posing $\epsilon_{\max} \equiv \dot{\omega}_{\max} \tau_{\max}^2$)

$$\alpha = \frac{1}{\tau_{\max}^2} - i\dot{\omega}_{\max} \equiv \frac{1}{\tau_{\max}^2} (1 - i\epsilon_{\max}), \quad \beta = i\omega_{\max}. \quad (42)$$

When \bar{t}' gets positive and large with respect to τ_{\max} (so that \bar{t}' is effectively $\sim +\infty$), we can estimate the total integrated recoil using the standard complex Gaussian integral:

$$\int_{-\infty}^{+\infty} dy e^{-\frac{1}{2}\alpha y^2 + \beta y} = \sqrt{2\pi} \frac{e^{\frac{1}{2}\frac{\beta^2}{\alpha}}}{\sqrt{\alpha}}. \quad (43)$$

This yields, for the modulus of the corresponding total integrated recoil

$$|v_{\text{com}}^x + i v_{\text{com}}^y| \simeq \sqrt{2\pi} \mathcal{F}_{\mathbf{P}}^{\max} \frac{\tau_{\max}}{(1 + \epsilon_{\max}^2)^{1/4}} e^{-\frac{1}{2}\frac{\omega_{\max}^2 \tau_{\max}^2}{1 + \epsilon_{\max}^2}}. \quad (44)$$

This approximate analytical result vividly illustrates the preceding discussion. Indeed, if the evolution of $\mathcal{F}_{\mathbf{P}}(t)$ were adiabatic ($Q \equiv \omega_{\max} \tau_{\max} \gg 1$) the total integrated recoil would be exponentially small (even if $\mathcal{F}_{\mathbf{P}}^{\max}$ gets large).

We have already indicated above, see Eq. (37), how one can analytically determine the location on the r -axis of the maximum of $\mathcal{F}_{\mathbf{P}}$. By analytically expanding Eq. (37) around its maximum, one can also get an analytical expression for the product $\tau_{\max} \dot{r}_{\max}$. As the reasoning above also gave the variation with r of the angular frequency, namely, $\omega(r)/\omega_{LSO} \approx [A(r)/r^2]/[A(r_{LSO})/r_{LSO}^2]$, we can obtain analytical estimates of ω_{\max} and of $\dot{\omega}_{\max}/\dot{r}_{\max}$. Finally, to get analytical estimates of all the quantities entering Eq. (44) we need an analytical estimate of \dot{r} around $r = r_{\max}$. This can be obtained (though only with modest accuracy) by using again the zero-damping approximation to write that the energy is approximately conserved during the plunge: hence

$$A(r) \left[1 + p_r^2/B(r) + p_\varphi^2/r^2 \right] \approx w_{LSO}, \quad (45)$$

with $w_{LSO} \approx A(r_{LSO})(1 + p_{\varphi_{LSO}}^2/r_{LSO}^2)$. Eq. (45) approximately determines the value of p_r during the plunge. From it, one then deduces the value of \dot{r} by using the Hamilton equation, Eq. (17a). See Fig. 4 of Ref. [8] for a plot of \dot{r} during the plunge.

These analytical approximations allows one to obtain estimates for all the quantities entering the crucial Eq. (44), and thereby to obtain an analytical estimate of the expected total recoil velocity v_{com} . We found that the results agrees within a few percent with the numbers one can extract from our full numerical simulations. The complete set of relevant quantities, extracted from our simulations, for the behavior around the time where $|\mathcal{F}_{\mathbf{P}}|$ reaches its maximum value are (for $\eta = 0.2$): $r_{\max} \simeq 3.501$, $\dot{r}_{\max} \simeq -0.113$, $\omega_{\max} \simeq 0.1255$, $\dot{\omega}_{\max} \simeq 2.952 \times 10^{-3}$, $|\mathcal{F}_{\mathbf{P}}|_{\max} \simeq 2.039 \times 10^{-5}$, $|\ddot{\mathcal{F}}_{\mathbf{P}}|_{\max} \simeq 3.683 \times 10^{-7}$, $\tau \simeq 7.440$, $Q \simeq 0.9337$, $\epsilon \simeq 0.1634$, and $\psi \simeq 1.007$. Of particular importance is the value of the quality factor, namely, $Q \simeq 0.9337$. The fact that it is of order unity means that a net integrated recoil is acquired soon after $\mathcal{F}_{\mathbf{P}}(t)$ reaches its maximum value, i.e. soon after the plunge has fallen below $r \simeq 3.501$, and therefore *before* reaching the light ring radius $r_{\text{lr}} = 3$.

Finally, we can analytically estimate, using Eq. (44), the final recoil that one might expect. We find

$$|v_{\text{com}}^x + i v_{\text{com}}^y|^{\text{integrated}} \simeq 74.06 \frac{f(\eta)}{f(0.2)} \tilde{F}_{\max} \text{ km/s}, \quad (46)$$

where we recall that $f(0.2) = 0.0178885$, the maximum value reached by $f(\eta)$ (when $\eta =$

0.2), and where \tilde{F}_{\max} denotes the value of the 2PN correction factor at $r = r_{\max} \simeq 3.501$. By definition, the quasi-Newtonian estimate corresponds to taking $\tilde{F} \equiv 1$.

IV. TRANSITION FROM PLUNGE TO RING-DOWN, AND GRAVITATIONAL RECOIL DURING RING-DOWN

Though the analytical estimate, given by Eq. (44), is interesting by the physical information it conveys [effect dominated by the maximum of $\mathcal{F}_{\mathbf{P}}(t)$, dependence on $f(\eta)$ and \tilde{F}_{\max} , and the obtainment of a small pure number from high powers of numbers “of order unity”], let us hasten to add that it is only an approximation to the real terminal recoil. Indeed, the above estimate, was obtained by taking the formal limit $\bar{t} \rightarrow +\infty$ in the truncated Gaussian integral, Eq. (41). However, as we have already indicated in the introduction, the physics behind the approximate analytical formulas, Eqs. (12), (14), or (18), changes when r reaches the “light ring” $r \simeq 3$. Following the analogous estimate of complete waveforms in Ref. [8], we propose here to estimate the contribution to the recoil due to the merger of black holes by formally terminating the plunge when the scaled radial coordinate gets around $r \simeq 3$, and by matching there the relevant time derivatives of the radiative multipole moments during the late plunge phase to corresponding “ring-down” multipole moments, constructed from appropriate quasi-normal mode contributions.

Let us first discuss why it is important to ensure as smooth a matching as possible during the transition from plunge to ring-down. To see this, let us consider again the approximate form of the final recoil velocity, given by Eq. (34), but let us now divide the full time interval in two phases: an inspiral + plunge phase, lasting from $t = -\infty$ up to some t_{match} , followed by a ring-down phase, lasting from t_{match} up to $t = +\infty$. The total recoil will be the sum of two contributions of the form ⁹

$$\mathcal{I}_{\text{plunge}} = \int_{-\infty}^{t_{\text{match}}} dt (a(t) e^{i\varphi(t)})|_{\text{plunge}}; \quad \mathcal{I}_{\text{ring}} = \int_{t_{\text{match}}}^{+\infty} dt (a(t) e^{i\varphi(t)})|_{\text{ring}}. \quad (47)$$

We now focus on the contribution to $\mathcal{I}_{\text{tot}} = \mathcal{I}_{\text{plunge}} + \mathcal{I}_{\text{ring}}$ that is formally linked to any “mismatch” between the two behaviors of the linear momentum flux around $t = t_{\text{match}}$, i.e. to any discontinuity between $i \left(\mathcal{F}_{\mathbf{P}}^{x\text{plunge}} + i \mathcal{F}_{\mathbf{P}}^{y\text{plunge}} \right) = [a(t) e^{i\varphi(t)}]_{\text{plunge}}$, considered for

⁹ Actually, the integral during the ring-down phase is a sum of terms $\propto e^{+i\varphi}$ and $e^{-i\varphi}$. See discussion below.

$t < t_{\text{match}}$, and $i \left(\mathcal{F}_{\mathbf{P}}^{\text{ring}} + i \mathcal{F}_{\mathbf{P}}^{\text{yring}} \right) = [a(t) e^{i\varphi(t)}]_{\text{ring}}$, considered for $t > t_{\text{match}}$. The effect of any discontinuity around $t = t_{\text{match}}$ can be obtained by summing the “edge contributions” of the two semi-infinite integrals, Eq. (47), i.e. the contributions linked to the upper or lower cut-off $t = t_{\text{match}}$. These “edge contributions” have been worked out in Ref. [38] to next-to-leading order in “adiabaticity expansion” [i.e. in powers of the formal small parameter ϵ , introduced in Eq. (34) above, by replacing $e^{i\varphi}$ by $e^{i\varphi/\epsilon}$], by using the “integration by parts” technique introduced above for showing that, in the absence of any discontinuity, the integral $\mathcal{I}(\epsilon) = \int dt a(t) e^{i\varphi(t)/\epsilon}$ vanishes faster than any power of ϵ . Adding two terms of the type of Eq. (3.17) in Ref. [38], the total edge contribution is of the form

$$\mathcal{I}_{\text{plunge}}^{\text{edge}} + \mathcal{I}_{\text{ring}}^{\text{edge}} = \left[\frac{a(t)}{i \dot{\varphi}(t)} e^{i\varphi(t)} \left\{ 1 + \frac{1}{i \dot{\varphi}(t)} e^{i\varphi(t)} \left[\frac{\ddot{\varphi}(t)}{\dot{\varphi}(t)} - \frac{\dot{a}(t)}{a(t)} \right] \right\} \right]_{\text{ring}}^{\text{plunge}}, \quad (48)$$

where the square bracket $\left[\mathcal{F}(a(t), \varphi(t), \dot{\varphi}(t), \dots) \right]_{\text{ring}}^{\text{plunge}}$ on the right-hand side of the above equation denotes the *difference*, $\mathcal{F}(a_{\text{plunge}}(t_{\text{match}}), \varphi_{\text{plunge}}(t_{\text{match}}), \dot{\varphi}_{\text{plunge}}(t_{\text{match}}), \dots) - \mathcal{F}(a_{\text{ring}}(t_{\text{match}}), \varphi_{\text{ring}}(t_{\text{match}}), \dot{\varphi}_{\text{ring}}(t_{\text{match}}), \dots)$. This analytical result highlights the following fact: any discontinuity between the amplitude, the phase, or any of their time-derivatives across t_{match} will contribute to the final recoil velocity. Therefore, if we want to minimize the *spurious* effects linked to our describing the smooth transition between the plunge and the merger by a fictitious sharp transition happening at $t = t_{\text{match}}$, we should try to match as many derivatives as possible of $\mathcal{F}_{\mathbf{P}} \propto a(t) e^{i\varphi(t)}$ across $t = t_{\text{match}}$. On the other hand, we are going to see that, even after having matched as well as possible $\mathcal{F}_{\mathbf{P}}$ across $t = t_{\text{match}}$, there remains a (non-spurious) “edge” contribution linked to the physical change of behavior across $t = t_{\text{match}}$.

To see this, let us consider in more detail how one can implement a physically motivated matching across $t = t_{\text{match}}$ (corresponding to $r_{\text{match}} \simeq 3$). All the physical effects which are important for the present study (flux of energy related to \mathcal{F}_{φ} , and flux of linear momentum, $\mathcal{F}_{\mathbf{P}}$) can be expressed as integrals over a sphere at infinity with integrands proportional to the local gravitational wave energy flux $\frac{dE}{d\Omega dt} = r^2 T_{00}^{\text{GW}} \propto \left(r \dot{h}_{ij} \right)^2$, where h_{ij} is the TT-gauge dimensionless gravitational wave amplitude, and \dot{h}_{ij} is its time derivative $\frac{\partial h_{ij}}{\partial t}$ [see, for e.g., Ref. [15]]. This motivates us to try to match as well as possible the quantity $r \dot{h}_{ij}(t, r, \theta, \phi)$, where θ and ϕ are polar angles on the sphere at infinity, between plunge and ring-down. The “radiative multipole moments” that enter the multipole expansion of $r \dot{h}_{ij}$ are, by definition,

the $(l + 1)$ -th time derivatives of the l -th mass (I^{lm}) and spin (or current) (S^{lm}) multipole moments ¹⁰. It is therefore most natural to match $I^{(l+1)lm}$ and $S^{(l+1)lm}$ across $t = t_{\text{match}}$. For the evaluation of $\mathcal{F}_{\mathbf{P}}$ at the leading order, the relevant radiative moments, as seen in Eq. (9), are $I^{(3)\pm 2}$; $S^{(3)\pm 1}$; $I^{(4)\pm 1}$ and $I^{(4)\pm 3}$. These terms correspond to gravitational waves, emitted by the two black holes, of multipolarity: ($l = 2, m = \pm 2$, even parity); ($l = 2, m = \pm 1$, odd parity); ($l = 3, m = \pm 1$, even parity); ($l = 3, m = \pm 3$, even parity), respectively. As a first approximation ¹¹, we can consider that these gravitational waves propagate (for radii larger than the radial distance $r(t)$ separating the two black holes) on a Schwarzschild background, of mass $M_S = E_{\text{tot}}^{\text{real}} \sim M \equiv m_1 + m_2$, approximately representing the (physical) spacetime outside the two holes. Therefore, when $r(t)$ gets smaller than about 3, the relevant modes $\dot{h}_{ij}^{l,m}$ will be strongly filtered by the corresponding Regge-Wheeler-Zerilli effective potential $V_{lm}^{(\text{even/odd})}(r)$. This filtering can be approximated by saying that, when the source of a mode (l, m, π) , where π denotes the parity, falls below $r = 3$, the corresponding outgoing wave mode can be described by a superposition of quasi-normal modes (QNM's) of the same multipolarity (l, m, π) .

Several nice simplifying features of gravitational wave propagation on a Schwarzschild background are that: (i) the effective potential $V_l^\pi(r)$ does not depend on the ‘‘magnetic quantum number’’, m , (ii) $V_l^\pi(r)$ is real, and (iii) though $V_l^{\text{even}} \neq V_l^{\text{odd}}$, they have the same spectrum of QNM complex frequencies [for a review of QNM's see Ref. [41]]. For each value of the multipolar order l , there is a double infinite sequence of QNM complex frequencies, say

$$\sigma_{ln}^\pm = \alpha_{ln} \pm i \omega_{ln}, \quad (49)$$

where $n = 0, 1, 2, \dots$, and α_{ln} and ω_{ln} are both real and positive [so that $\sigma_{ln}^+ \equiv (\sigma_{ln}^-)^*$]. The notation here is that the n -th QNM mode belonging to the multipolarity l decays, when $t \rightarrow +\infty$, proportionally to $e^{-\sigma_{ln}^\pm t} = e^{-\alpha_{ln} t} e^{\mp i \omega_{ln} t}$. For each value of l the fundamental QNM mode $n = 0$ is the least-damped one, i.e. the one with the smallest value for α_{ln} .

¹⁰ For simplicity, we use here the nomenclature of Ref. [15]. In the multipolar post-Minkowskian formalism, Refs. [24, 25, 26, 27, 28, 29, 30, 31, 32], the ‘‘radiative’’ moments are defined as $U^{lm} \sim I^{(l)lm}$ and $V^{lm} \sim S^{(l)lm}$, i.e. as the moments entering the multipole expansion of $r h_{ij}$. In the latter nomenclature, the moments that most directly enter the quantities that we need would be \dot{U}^{lm} and \dot{V}^{lm} (and would include all required ‘tail’ effects).

¹¹ We leave to future work the refinement consisting in using modes propagating over a Kerr background.

Finally, our matching procedure consists in joining, as smoothly as possible, across $t = t_{\text{match}}$, each relevant multipolar mode entering $r \dot{h}_{ij}^{l,m}$, namely, $I_{\text{plunge}}^{2\pm 2(3)}(t)$, $S_{\text{plunge}}^{2\pm 1(3)}(t)$, $I_{\text{plunge}}^{3\pm 1(4)}(t)$, and $I_{\text{plunge}}^{3\pm 3(4)}(t)$, obtained for $t < t_{\text{match}}$ by differentiating Eqs. (11) in the quasi-circular approximation ($\dot{r} \ll r \dot{\phi}$), to corresponding ‘‘ring down’’ multipole moments, made of sum of decaying QNM modes. For instance, this leads (after scaling out the total mass M) to matching

$$I_{\text{plunge}}^{22(3)}(t) = i \frac{16}{5} \sqrt{10} \pi \eta r(t)^2 \omega(t)^3 e^{-2i\varphi(t)} \quad (\text{for } t < t_{\text{match}}), \quad (50)$$

where $r(t), \varphi(t), \omega(t) = \dot{\varphi}(t)$ are obtained by numerically integrating the EOB dynamics, Eqs. (17), to a corresponding ‘‘ring down’’ radiative moment of the form

$$I_{\text{ring}}^{22(3)}(t) = \sum_{n=0,1,\dots} \left\{ C_n^+(I^{22}) e^{-\sigma_{2n}^+ \tau} + C_n^-(I^{22}) e^{-\sigma_{2n}^- \tau} \right\} \quad (\text{for } \tau \equiv t - t_{\text{match}} > 0), \quad (51)$$

where σ_{2n}^\pm , $n = 0, 1, \dots$, are the QNM frequencies, Eq. (49), belonging to the multipolarity $l = 2$, and where $C_n^\pm(I^{22})$ denotes, for each n , two independent complex coefficients. Indeed, $I_{\text{ring}}^{22(3)}(t)$ being complex, there are no reality conditions relating $C_n^+(I^{22})$ and $C_n^-(I^{22})$ (in spite of the fact that σ_{2n}^+ and σ_{2n}^- are related by complex conjugation).

If we include in Eq. (51) only the first two complex conjugated fundamental QNM modes, σ_{20}^+ and σ_{20}^- , we observe that $I_{\text{ring}}^{22(3)}(t)$ contains two arbitrary complex coefficients $C_0^+(I^{22})$ and $C_0^-(I^{22})$. These two complex coefficients can be chosen so as to ensure not only that $I_{\text{plunge}}^{22(3)}(t = t_{\text{match}})$ agrees with $I_{\text{ring}}^{22(3)}(t = t_{\text{match}}) = C_0^+(I^{22}) + C_0^-(I^{22})$, but also that the (numerically computed¹²) time derivative $\frac{dI_{\text{plunge}}^{22(3)}(t)}{dt}$ agrees, when $t = t_{\text{match}}$ with $\frac{dI_{\text{ring}}^{22(3)}(t)}{dt} = -\sigma_{20}^+ C_0^+(I^{22}) - \sigma_{20}^- C_0^-(I^{22})$. This yields

$$C_0^+(I^{22}) = \frac{\left[\sigma_{20}^- I_{\text{plunge}}^{22(3)}(t) + \frac{dI_{\text{plunge}}^{22(3)}(t)}{dt} \right]_{t=t_{\text{match}}}}{\sigma_{20}^- - \sigma_{20}^+}, \quad (52a)$$

$$C_0^-(I^{22}) = \frac{\left[\sigma_{20}^+ I_{\text{plunge}}^{22(3)}(t) + \frac{dI_{\text{plunge}}^{22(3)}(t)}{dt} \right]_{t=t_{\text{match}}}}{\sigma_{20}^+ - \sigma_{20}^-}. \quad (52b)$$

¹² For a smooth match, one should no longer use the quasi-circular approximation, $\dot{r} \ll r \dot{\phi}$, when computing the time derivatives of $I_{\text{plunge}}^{22(3)}(t)$.

Similarly, we can match, in a once-differentiable (C^1) manner, $S_{\text{plunge}}^{21(3)}(t)$, $I_{\text{plunge}}^{31(4)}(t)$, and $I_{\text{plunge}}^{33(4)}(t)$ to ring down moments of the form

$$S_{\text{ring}}^{21(3)}(t) = C_0^+(S^{21}) e^{-\sigma_{20}^+ \tau} + C_0^-(S^{21}) e^{-\sigma_{20}^- \tau}, \quad (53a)$$

$$I_{\text{ring}}^{31(4)}(t) = C_0^+(I^{31}) e^{-\sigma_{30}^+ \tau} + C_0^-(I^{31}) e^{-\sigma_{30}^- \tau}, \quad (53b)$$

$$I_{\text{ring}}^{33(4)}(t) = C_0^+(I^{33}) e^{-\sigma_{30}^+ \tau} + C_0^-(I^{33}) e^{-\sigma_{30}^- \tau}. \quad (53c)$$

Each pair of complex coefficients $C_0^\pm(\mathcal{M})$ is then given as a linear combination of $\mathcal{M}_{\text{plunge}}(t_{\text{match}})$ and $\frac{d}{dt}\mathcal{M}_{\text{plunge}}(t_{\text{match}})$ of the type, given by Eq. (52) above. Finally, we can use the complex conjugation relations, Eq. (10), to match, in a C^1 manner, the remaining required radiative moments $I^{2-2(3)}(t)$ and $I^{3-3(4)}(t)$ entering Eq. (9). This does not introduce new, independent coefficients as

$$(-)^m C_0^\pm(I^{lm}) = C_0^\pm[(I^{lm})^*] = [C_0^\mp(I^{lm})]^*. \quad (54)$$

Note also that to match the multipole moments entering the leading order linear momentum flux, we need to know only two conjugate pairs of complex QNM frequencies, namely from Refs. [42] and [41],

$$\sigma_{20}^\pm = 0.08896 \pm 0.37367 i, \quad (55a)$$

$$\sigma_{30}^\pm = 0.09270 \pm 0.59944 i. \quad (55b)$$

Having so determined continuations of the various relevant multipole moments during the merger phase, we get an estimate of the final recoil, in the leading-order (quasi-Newtonian) approximation by integrating, from $-\infty$ to t_{match} and then from t_{match} to $+\infty$, the linear momentum balance equation

$$\frac{d}{dt}(v_{\text{com}}^x + i v_{\text{com}}^y) = -\frac{1}{336 \pi} \left\{ \sqrt{14} I^{2-2(3)} I^{31(4)} + \sqrt{210} I^{22(3)} I^{3-3(4)} - 14 i I^{2-2(3)} S^{21(3)} \right\}. \quad (56)$$

Here the ‘‘radiative moments’’ $I^{(l+1)lm}$ and $S^{(l+1)lm}$ appearing on the right-hand side (RHS) are given by: (i) when $t < t_{\text{match}}$ by Eq. (50) and similar ‘‘plunge moments’’ $I_{\text{plunge}}^{(l+1)lm}$, $S_{\text{plunge}}^{(l+1)lm}$ obtained by differentiating (while neglecting $\dot{r} \ll r \dot{\varphi}$) Eqs. (11), and (ii) when $t > t_{\text{match}}$ by analytical QNM-based ‘‘ring-down moments’’ $I_{\text{ring}}^{(l+1)lm}$, $S_{\text{ring}}^{(l+1)lm}$, defined by Eqs. (53) above. The C^1

continuity of the moments entering the RHS of Eq. (56) ensures that the linear momentum flux $\mathcal{F}_{\mathbf{P}}$ [defined by the RHS of Eq. (56)] is continuous, as well as its first derivative, across $t = t_{\text{match}}$.

As explained above this C^1 matching ensures that one did not introduce leading-order spurious contributions linked to edge effects. At the same time, this matching procedure generically introduces discontinuities in the second time derivative of $\mathcal{F}_{\mathbf{P}}$. We then see from Eq. (48) that there will be sub-leading spurious contributions linked to such discontinuities in $\frac{d^2\mathcal{F}_{\mathbf{P}}}{dt^2}$. To study the eventual numerical importance of these higher-order edge effects, we have also implemented an improved matching procedure consisting of including, for each radiative multipole moment, the first two conjugate pairs of QNMs in Eq. (51), i.e. both $n = 0$ (fundamental QNMs) and $n = 1$ (first excited QNMs). The new required QNM frequencies, available in Refs. [41, 42], are

$$\sigma_{21}^{\pm} = 0.27391 \pm i 0.34671, \quad (57a)$$

$$\sigma_{31}^{\pm} = 0.28130 \pm i 0.58264. \quad (57b)$$

As the QNM sums, Eq. (51), now include 4 arbitrary complex coefficients $C_0^+, C_0^-, C_1^+, C_1^-$, we can uniquely determine them by demanding that each radiative moments (say I^{22}), together with their first *three* numerically computed time derivatives ($\frac{d^j I^{22}}{dt^j}$ for $j \leq 3$) match across t_{match} .

The matching procedure presented so far was based on considering the leading-order, quasi-Newtonian, expression, Eq. (9), for the flux of linear momentum. When considering the 2PN correction factor \tilde{F} , as in Eq. (18), we should, in principle, both include more multipolarities in Eq. (9), and PN-corrections in the expressions for individual radiative moments, Eqs. (11) or Eq. (50). As we found (see below) that contributions to the recoil due to the ring-down phase are relatively small, we decided, for simplicity, to use a less-rigorous, but much simpler, 2PN-level matching procedure. The procedure we used consisted in continuing to use the leading-order flux, as in Eq. (9), but to “improve” the “brick radiative moments”, I^{2m}, S^{2m}, I^{3m} , it contains by multiplying each of them by a factor $\sqrt{\tilde{F}}$, e.g. we modify Eq. (50) to

$$I_{\text{plunge}}^{22(3)\text{ improved}} = i \sqrt{\tilde{F}} \frac{16}{5} \sqrt{10\pi} \eta r(t)^2 \omega(t)^3 e^{-2i\varphi(t)} \quad (\text{for } t < t_{\text{match}}). \quad (58)$$

Then we match each of these “improved plunge moments” to a corresponding “ring-down” one, given by a QNM sum of the form, given by Eqs. (51). Again this matching can be done in a C^1 (2 QNM’s) or C^3 (4 QNM’s) manner.

V. RESULTS

Having presented our methodology, let us now discuss the results that we obtained, and their interpretation. Let us consider first the leading-order, quasi-Newtonian approximation, i.e. Eqs. (12) and (14), together with the leading-order (2 QNM’s per moment) matching to the ring-down phase. We plot in Fig. 4, for the case of $\eta = 0.2$, the magnitude of the linear momentum flux $|\mathcal{F}_{\mathbf{P}}^i|$, together with their two separate components $\mathcal{F}_{\mathbf{P}}^x$ and $\mathcal{F}_{\mathbf{P}}^y$, as functions of time. The maximum of $|\mathcal{F}_{\mathbf{P}}^i|$ is reached for $t = t_{\max} \simeq 4149.50$ (which corresponds to $r_{\max} \simeq 3.501$, in an evolution for which the initial separation when $t = 0$ was $r = 15$, while the matching to the ring-down phase was done at $t = t_{\text{match}} \simeq 4153.50$, which corresponds to $r_{\text{match}} \simeq 2.933$. Note the rather fast (and oscillatory) decay of the individual components of $\mathcal{F}_{\mathbf{P}}^i$ during the ring-down. Indeed, we see from Eqs. (51) to (53) that, during the ring-down, $\mathcal{F}_{\mathbf{P}}^i$ is a sum of contributions proportional either to $e^{-(\sigma_{20}^{\epsilon_2} + \sigma_{30}^{\epsilon_3})\tau} = e^{-(\alpha_{20} + \alpha_{30})\tau} e^{-i(\epsilon_2 \omega_{20} + \epsilon_3 \omega_{30})\tau}$ (where $\epsilon_2^2 = 1 = \epsilon_3^2$) or to $e^{-(\sigma_{20}^{\epsilon_2} + \sigma_{20}^{\epsilon_2'})\tau} = e^{-2\alpha_{20}\tau} e^{-i(\epsilon_2 + \epsilon_2')\omega_{20}\tau}$ (where $\epsilon_2^2 = 1 = \epsilon_2'^2$). From Eqs. (51) and (53), we see that the slowest exponential decay is $\propto e^{-2\alpha_{20}\tau}$, which decays on a characteristic time scale $\tau_{\text{ring}} = \frac{1}{2\alpha_{20}} \sim 5.62$. Though this is significantly smaller than the orbital period near the LSO, note, however, that this time scale is comparable both to the characteristic time scale for the variation of $\mathcal{F}_{\mathbf{P}}(t)$ near its maximum ($\tau_{\max} \simeq 7.440$, see above) and to the inverse of the angular frequency near the latter maximum ($\frac{1}{\omega_{\max}} \simeq \frac{1}{0.1255} \simeq 7.968$).

In Fig. 5, we display the temporal evolution of the recoil velocity, where we exhibit both its magnitude $|\mathbf{v}_{\text{com}}^i(t)|$ and its two separate components $\mathbf{v}_{\text{com}}^x(t)$ and $\mathbf{v}_{\text{com}}^y(t)$. We see that the maximum instantaneous recoil velocity is reached *after* the maximum of $|\mathcal{F}_{\mathbf{P}}|$, and while $|\mathcal{F}_{\mathbf{P}}|$ has already significantly decreased. After having reached its maximum value, $|\mathbf{v}_{\text{com}}^i(t)|$ slightly decreases, in general with some oscillations, before settling down to its terminal value (see top panel in Fig. 5). A useful visualization of the evolution of the recoil is provided by plotting the “hodograph”, i.e. a parametric plot of the instantaneous recoil velocity vector in the two-dimensional plane ($\mathbf{v}_{\text{com}}^x, \mathbf{v}_{\text{com}}^y$): see Fig. 6. The behavior of the instantaneous recoil

velocity is easily interpreted in view of the analytical arguments presented above. Indeed, we have seen in Eq. (44) that, during the plunge, the main contribution to the integrated recoil came from the *non-adiabatic* character of the evolution of $|\mathcal{F}_{\mathbf{P}}(t)|$ near its maximum. This led us to estimate that the instantaneous recoil $v_{\text{com}}(t)$ was given by the truncated Gaussian integral, Eq. (41). This integral can be expressed by a (complementary) error function $\text{erfc}(z) = \left(\frac{2}{\sqrt{\pi}}\right) \int_z^{+\infty} e^{-x^2} dx$, with argument $z = -\sqrt{\frac{\alpha}{2}} \left(\bar{t} - \frac{\beta}{\alpha}\right)$ where $\bar{t} \equiv t - t_{\text{max}}$, and where α and β are defined by Eq. (42). If, for simplicity, one neglect $\epsilon_{\text{max}} \ll 1$, we find that $z \sim -\frac{1}{\sqrt{2}} \left(\frac{\bar{t}}{\tau_{\text{max}}} - i\omega_{\text{max}} \tau_{\text{max}}\right)$. Note that z is shifted (by a quantity of order unity because $\omega_{\text{max}} \tau_{\text{max}} = Q \simeq 0.9337$) in the complex plane. This shift in the complex plane introduces some modifications to the usual behavior of the complementary error function in the real domain, which evolves monotonically from $\text{erfc}(+\infty) = 0$ when $z = +\infty$, i.e. $\bar{t} = -\infty$, to $\text{erfc}(-\infty) = 2$ when $z = -\infty$, i.e. $\bar{t} = +\infty$. These modifications are such that the modulus $|\text{erfc}(z(\bar{t}))|$ increases from the value 0 when $\bar{t} = -\infty$ to a maximum value of about 2.05 when $\frac{\tau}{\tau_{\text{max}}} \simeq +1.06$, before decreasing toward its final value of 2 when $\frac{\tau}{\tau_{\text{max}}} \gg 1$. Note also that $|\text{erfc}(z(\bar{t}))|$ already reaches the value $\simeq 1.97$ when $\frac{\tau}{\tau_{\text{max}}} \simeq +1$. Therefore, most of the integrated effect of the maximum of $|\mathcal{F}_{\mathbf{P}}(t)|$ is acquired when $t - t_{\text{max}} \sim +\tau_{\text{max}}$. However, in the case of the evolution depicted in Fig. 2, one can check that the time $t_{\text{max}} + \tau_{\text{max}}$ corresponds to a radius $r \simeq 2.648$, which is (slightly) below $r \simeq 3$, i.e. after our chosen transition time to ring-down $t_{\text{match}} \simeq 4153.5$ (corresponding to $r \simeq 2.933$). Therefore, the integrated effect up to t_{match} of the non-adiabatic evolution of $|\mathcal{F}_{\mathbf{P}}(t)|$ near its maximum will be slightly smaller than the total integrated effect considered above.

In addition, the transition from $\mathcal{F}_{\mathbf{P}}^{\text{plunge}}(t)$ to $\mathcal{F}_{\mathbf{P}}^{\text{ring}}(t)$ across t_{match} introduces a new source of non-adiabaticity¹³. Fig. 5 shows that the ring-down behavior can introduce some oscillations in $|\mathbf{v}_{\text{com}}|$, and tends to *decrease* the value of $|\mathbf{v}_{\text{com}}|$ reached after passing the maximum of $|\mathcal{F}_{\mathbf{P}}|$. However, one sees on the plot that the effect of ring-down is relatively small compared to the main contribution to $|\mathbf{v}_{\text{com}}|$ acquired by passing over the maximum of $|\mathcal{F}_{\mathbf{P}}(t)|$. The relative smallness of the ring-down contribution to $|\mathbf{v}_{\text{com}}|$ can also be checked analytically. Indeed, this ring-down contribution is given by a sum of integrals of the form $\int_0^{+\infty} d\tau \mathcal{C} e^{-(\alpha+i\omega)\tau} = \frac{\mathcal{C}}{\alpha+i\omega}$. One can then relate this sum of integrals to the value of $|\mathcal{F}_{\mathbf{P}}|$

¹³ The non-adiabatic character of the transition between plunge and ring-down shows up particularly in the fact that one passes from a quasi-monochromatic (chirping) form $[\mathcal{F}_{\mathbf{P}}^x(t) + i\mathcal{F}_{\mathbf{P}}^y(t)]_{\text{plunge}} = a(t) e^{i\varphi(t)}$ to a non-monochromatic form containing both (decaying) positive and negative frequencies: $e^{\alpha\tau} e^{\pm i\omega\tau}$.

at the moment of the matching. One then checks that, because the transition occurs while $|\mathcal{F}_{\mathbf{P}}|$ has already significantly decreased from its maximum value, the ring-down integral will be significantly smaller than the value acquired by passing over the maximum of $|\mathcal{F}_{\mathbf{P}}(t)|$.

In Figs. 7 and 8, we study the effect of demanding a smoother transition between plunge and ring-down, namely a C^3 one (with two conjugate pairs of QNM's per multipole moments) instead of the C^1 one (one pair of QNM's) used in the Figs. 4 and 5. As we see, though the effect is not negligible (and can introduce some extra oscillations in $\mathbf{v}_{\text{com}}^i$), it has a relatively minor effect on the final recoil velocity. More precisely, we find that (for $\eta = 0.2$) $v_{\text{com}}^{\text{terminal}}|_{2 \text{ QNM}} \simeq 51.05$ km/s, while $v_{\text{com}}^{\text{terminal}}|_{4 \text{ QNM}} \simeq 54.19$ km/s.

Let us now consider the impact on $v_{\text{com}}^{\text{terminal}}$ of the higher-order PN corrections to $\mathcal{F}_{\mathbf{P}}$, i.e. the effect of the factor \tilde{F} in Eq. (18). The definition of \tilde{F} , given by Eq. (25), depends on the definition of $F(v)^{14}$. We have discussed above various ways of estimating F : one can use straightforward ‘‘Taylor approximants’’, (e.g. $F_{1PN}^T \equiv 1 + F_2 v^2$), or, instead, some ‘‘Padé’’ ones (e.g. $F_{1PN}^P = \frac{1}{1 - \frac{v}{v_{\text{pole}}}} \frac{1}{1 + \frac{c_1 v}{1 + c_2 v}}$). Actually, the 1PN-accurate Taylor approximant $F_{1PN}^T \equiv 1 + F_2 v^2$ is not an acceptable approximation for the study of the recoil. Indeed, when $\eta = 0.2$, one finds that F_{1PN}^T becomes *negative* for $v \geq 0.421$. As $v_{\varphi} = \omega r$ is about 0.44 at the maximum of $\mathcal{F}_{\mathbf{P}}$, the most important domain of values for v_{φ} to estimate the recoil would correspond to such a physically incorrect negative value for F_{1PN}^T . Though the corresponding Padé approximant F_{1PN}^P stays positive, it is also unphysical in that it takes values of order 10 in the relevant range of values for v . Therefore, we shall only consider the higher-order PN approximants: $F_{1.5PN}^T$, F_{2PN}^T , $F_{1.5PN}^P$, and F_{2PN}^P . In Table I, we present (for $\eta = 0.2$), the values of $|\mathbf{v}_{\text{com}}|$, $\mathbf{v}_{\text{com}}^x$, and $\mathbf{v}_{\text{com}}^y$ for various approximants and at various stages of the inspiral or merger. We observe that changing the approximant for \tilde{F} has a substantial effect on v_{com} . In particular, the final recoil varies between $v_{\text{com}}^{\text{terminal}} \simeq 50$ km/s when using a 2PN accurate Padé approximant, and $v_{\text{com}}^{\text{terminal}} \simeq 74$ km/s with a 2PN accurate Taylor approximant (the quasi-Newtonian estimate being $v_{\text{com}}^{\text{terminal}} \simeq 51$ km/s). In agreement with the approximate analytical estimate derived above, one can check that $v_{\text{com}}^{\text{terminal}}$ varies in direct proportion to the value taken by the PN factor \tilde{F} at $t = t_{\text{max}}$, i.e. when $|\mathcal{F}_{\mathbf{P}}(t)|$ reaches its maximum value. Indeed, neglecting the effect of ψ in Eq. (25) [$\psi(t_{\text{max}}) \sim 1.007$], the variation of

¹⁴ For simplicity, in view of the closeness of $\psi(r, p_{\varphi})$ to 1, we shall not contemplate other definitions of \tilde{F} based, e.g., on expanding *both* ψ and F in PN series before, eventually re-summing the PN expansion of \tilde{F} .

$v_{\text{com}}^{\text{terminal}}$ with F is well describable by the variation of $F(v_{\text{max}})$ with $v_{\text{max}} \simeq 0.439$. Indeed, we have the following values for F , namely, $F_N(v_{\text{max}}) = 1$, $F_{1.5PN}^T(v_{\text{max}}) \simeq 1.33$, $F_{2PN}^T(v_{\text{max}}) \simeq 1.35$, $F_{1.5PN}^P(v_{\text{max}}) \simeq 1.27$, and $F_{2PN}^P(v_{\text{max}}) \simeq 0.93$ which are well correlated with the results listed in Table I. The significant difference between $F_{2PN}^T(v_{\text{max}})$ and $F_{2PN}^P(v_{\text{max}})$ illustrates again the poor convergence of the successive PN contributions. As argued earlier, one would expect [by analogy with convergence of the energy-flux function $F_E(v)$] that the 2.5 PN-accurate Padé approximant would yield a better answer. In absence of information concerning the 2.5 PN level, we shall use F_{2PN}^T as our best answer [in view of the behavior of $F_{E_{2PN}}^T$ [36]], but keep in mind the probability of a significant error bar around it.

In Table II, we study the influence of another parameter in our methodology: the precise choice of the transition radius between plunge and ring-down. We consider the standard Schwarzschild light ring, namely $r = 3$, as our default value. In Table II, we explore the effect on $v_{\text{com}}^{\text{terminal}}$ of changing the matching radius r_{match} by $\pm 20\%$ of its default value. As this Table shows, the value of $v_{\text{com}}^{\text{terminal}}$ is mildly sensitive to the precise choice of transition radius.

Up to now, we have only focused on a specific symmetric mass ratio ($\eta = 0.2$) which, in view of the analytical estimate, given by Eqs. (44) and (46), is expected to yield the maximum possible recoil. In Table III, we consider several different values of η , namely $\eta = 0.05, 0.1, 0.2$, and 0.24 and compute the corresponding *scaled* terminal recoil $\hat{v}_{\text{com}} = \frac{v_{\text{com}}}{f(\eta)}$, where $f(\eta) = \eta^2 \sqrt{1 - 4\eta}$. As expected, after scaling out the function $f(\eta)$, the recoil depends only weakly on η . We can analytically approximate the η -dependence of \hat{v}_{com} by a second-order polynomial $P(\eta) = a + b\eta + c\eta^2$. Normalizing a, b and c so that $P(0.2) = 1$, we find a reasonable fit¹⁵ for

$$P(\eta) = 1.0912 - 1.04\eta + 2.92\eta^2. \quad (59)$$

Finally, putting together the various informations we have obtained above, we can summarize our “best bet” estimate for the final recoil associated with the coalescence of binary black holes of symmetric mass ratio η as

$$v_{\text{com}}^{\text{final}} \simeq 73.5 \frac{\tilde{F}_{\text{max}}}{1.35} \hat{f}(\eta) \text{ km/s}, \quad (60)$$

¹⁵ Actually, to get a good fit to the data in Table III one needs a third-order polynomial, namely: $P_3(\eta) = 1.112 - 1.78\eta + 10.3\eta^2 - 21\eta^3$.

where $\hat{f}(\eta) = \frac{\eta^2 \sqrt{1-4\eta}}{0.0178885} (1.0912 - 1.04\eta + 2.92\eta^2)$. The fiducial value 1.35 used above for scaling \tilde{F}_{\max} is the prediction made by the 2PN Taylor approximant around $r_{\max} \simeq 3.50$, i.e. at the moment where the modulus of the linear momentum flux is maximum. Note that the proportionality of the final result to \tilde{F}_{\max} is only approximate because the presence of the correction factor $\tilde{F}(t)$ changes not only the height of the maximum of $|\mathcal{F}_{\mathbf{P}}|$ but also affects the shape of $|\mathcal{F}_{\mathbf{P}}|(t)$ and thereby the quality factor Q etc. The above estimate is plotted as a function of $q = \frac{m_2}{m_1}$ in Fig. 9.

VI. DISCUSSION

The main fruit of the present study is the fact that we have delineated, often by means of analytical arguments, the relative importance of several different physical effects in determining the magnitude of the final recoil velocity $v_{\text{com}}^{\text{final}}$. We have emphasized that the value of $v_{\text{com}}^{\text{final}}$ is essentially determined by a brief period during the orbital evolution when the integrand of the oscillatory integral (34) yielding $v_{\text{com}}^{\text{final}}$ varies in a non adiabatic manner: $\dot{a}/a \sim \dot{\varphi}$. We have found that this non-adiabatic evolution is confined to a small neighborhood of the moment, during the plunge, where the modulus of the linear momentum flux $|\mathcal{F}_{\mathbf{P}}|(t)$ [i.e. the amplitude $a(t)$ in the integral (34)] reaches a maximum. The good news is that it seems that this maximum takes place during the quasi-circular “plunge phase”, i.e. during a phase where the radial kinetic energy is significantly smaller than the azimuthal kinetic energy. Indeed, the ratio $\mathcal{R} \equiv g^{RR} p_R^2 / g^{\varphi\varphi} p_\varphi^2$ between “radial” and “azimuthal” kinetic energies is found to take the value $\mathcal{R}_{\max} \simeq 0.135$ at r_{\max} . [Note again, that even at the light ring, $r \simeq 3$ this ratio remains small, namely, $\mathcal{R}_{\text{lr}} \simeq 0.281$].

This “burst” of linear momentum flux also occurs slightly before the merger phase which we view as taking place when the (adimensionalized) radial distance r gets smaller than about 3. As was argued in Ref. [8] the quasi-circular “plunge” phase ($3 < r < 6$) is a priori amenable to analytical description within the EOB approach. And we have indeed checked that various different ways of completing the EOB approach by a suitable matching to a subsequent ($r < 3$) ring-down description of the merging of the two black holes did not affect much the recoil velocity acquired after passing over the maximum of $|\mathcal{F}_{\mathbf{P}}|(t)$. We have also verified that various other physical ingredients of the model (such as: the representation of the damping force during the plunge, the choice of matching point, the

number of quasi-normal modes, \dots) had a rather mild effect on the final recoil.

However, the bad news is that when $|\mathcal{F}_{\mathbf{P}}|(t)$ reaches its maximum value, the azimuthal kinetic energy contribution p_φ^2/r^2 in the Hamiltonian equations, Eqs. (17), as illustrated in Fig. 1, is of order unity ($p_\varphi^2/r_{\max}^2 \sim 1$), i.e. comparable to the constant term ($= 1$), which plays the role of the “squared rest mass” term in the Hamiltonian ($H \sim \sqrt{\mathbf{p}^2 + m^2}$). This situation contrasts with the one near the LSO, where one has $p_\varphi^2/r_{LSO}^2 \sim 0.25$ which is significantly smaller than unity. In other words, the orbital motion near the LSO is still “non relativistic” (by a thin margin), while the recoil is generated when the orbital motion becomes mildly relativistic (in the sense $\mathbf{p}^2 \sim m^2$). What further complicates the matter is that the orbital motion does not follow the usually considered sequence of circular orbits, so that we cannot use the standardly assumed relativistic version of Kepler’s third law relating the angular velocity to the radius. In the body of the paper, we have used the “quasi-Newtonian” expression for the linear momentum flux (in EOB coordinates) as a guideline to select a “best bet” modeling of $\mathcal{F}_{\mathbf{P}}(t)$ during the plunge. We have already seen in Table I that a very significant source of uncertainty in the magnitude of $\mathcal{F}_{\mathbf{P}}(t)$ concerns the inclusion of post-Newtonian corrections in it. Depending on whether one uses the straightforward “Taylor-expanded” 2PN correction [5], or one of its Padé-resummed versions, one gets a multiplicative factor varying between 0.92 and 1.35 in $v_{\text{com}}^{\text{final}}$. However, this uncertainty is only a *lower limit* to the total uncertainty currently attached to the description of the relativistic effects during the plunge. We can see hints of a larger uncertainty by comparing our EOB-based treatment (which did not assume the validity of the standard Kepler law during the plunge) to a treatment similar to the one advocated in Ref. [5] (which did implicitly assume the continued validity of Kepler’s law). To explore this issue, and also to understand the relation between our estimate and the significantly larger one obtained in Ref. [5], we have estimated the recoil following from using the functional form (3) for $\mathcal{F}_{\mathbf{P}}$, instead of our 2PN-corrected, quasi-Newtonian expression (18). As we discussed above, these two different functional forms can be matched above the LSO [modulo the suitable definition of the 2PN-correcting factor \tilde{F} in Eq. (18), see Eq. (25)], by using the relativistic Kepler law (21). On the other hand, Eq. (21) gets strongly violated below the LSO, and as a consequence the two different functional forms, Eqs. (3) and (18), a priori lead to quite different time evolutions for $\mathcal{F}_{\mathbf{P}}(t)$. In keeping with our general philosophy, it is useful to understand analytically the difference between the two basic corresponding “quasi-Newtonian” prescriptions [obtained

by neglecting the 2PN factor F in Eq. (3) and the corresponding 2PN factor \tilde{F} in Eq. (18)]. In other words, let us discuss the effect of replacing our basic “fiducial” quasi-Newtonian momentum flux $\mathcal{F}_{r,\omega} = r^5\omega^7$ by $\mathcal{F}_{v_\omega} = v_\omega^{11} = (\omega)^{11/3}$. Let us call $K \equiv \omega^2 r^3$ the quantity which is (approximately) constant when Kepler’s law is satisfied. It is then easy to see that the ratio between the two prescriptions reads: $\mathcal{F}_{v_\omega}/\mathcal{F}_{r,\omega} = K^{-5/3}$. We have shown above how to write an approximate evolution equation for the angular frequency during the plunge, namely: $\omega \propto A(r)/r^2$. This entails that K varies during the plunge approximately as $K \propto A^2(r)/r$. It can be analytically checked that K , or better $\hat{K} = \psi K$ with ψ defined by Eq. (22) (augmented by the needed p_r^2 terms), is equal to 1, and has a horizontal derivative, at the LSO, and *decreases* monotonically when $r < r_{LSO}$, to reach zero when r tends to the “horizon” [$A(r_{horizon}) = 0$]. This behavior is illustrated in Fig. 3. As a consequence K gets (significantly) smaller than 1 below the LSO, so that $\mathcal{F}_{v_\omega}/\mathcal{F}_{r,\omega} = K^{-5/3}$ is significantly larger than 1 during the plunge. More precisely, we can, as above, study the evolution of $\mathcal{F}_{v_\omega}(t)$ by writing that it approximately varies like $\mathcal{F}_{v_\omega} = [\omega(r)]^{11/3} \propto [A(r)/r^2]^{11/3}$. It can be seen that this function of r has a maximum at $r'_{\max} \approx 2.879$, and that the value of the function at its maximum is more than *twice* higher than the maximum that $\mathcal{F}_{r,\omega} = r^5\omega(r)^7$ had at $r_{\max} \approx 3.443$. This increase in the maximum value of the linear momentum flux is further compounded by significant changes in the shape of the maximum (notably the value of the crucial quality factor $Q \equiv \omega_{\max} \tau_{\max}$ introduced above). We therefore see that using a momentum flux given by Eq. (3) instead of Eq. (18) will more than *double* the value of $v_{\text{com}}^{\text{final}}$ [see precise numbers below]. Note that the large change in the predicted value for $v_{\text{com}}^{\text{final}}$ that we just discussed concerns only the “leading-order quasi-Newtonian” expression that one chooses to employ during the plunge. It has to be further compounded by the uncertainty linked to the resummation of the 2PN correction factor F or \tilde{F} (which brings a multiplicative uncertainty factor of order 1.5).

Actually, the fact that the location of the maximum of the momentum flux ($r'_{\max} \approx 2.879$) is slightly *below* the light ring in the case of Eq. (3) brings a further complication. Indeed, in that case we cannot trust our simple “Gaussian integral estimate” Eq. (44) which assumed that one was integrating over the maximum of $|\mathcal{F}_{\mathbf{P}}|(t)$. The matching to the subsequent ring-down behavior could a priori have a significant impact. To resolve this issue we have run numerical simulations similar to what we use in the body of the paper (with EOB dynamics as defined above, and two Quasi-Normal-Modes matching at $r = 3$) except that

the right-hand side of Eq. (18) was replaced by Eq. (3). Our results are displayed in Fig. 10 and listed in the last two rows of Table I. In agreement with the simple analytic arguments above, we do find final recoil velocities that are more than twice larger when using Eq. (18) (with a corresponding factor \tilde{F}). For instance, from Fig. 10, we find that the terminal recoil is ~ 172 km/s which is more than double the value that we read in the Table I for a 2PN accurate \tilde{F} . Furthermore, using Eq. (3) as it stands we observe, for the optimal case $\eta = 0.2$ and while terminating the EOB evolution at $r \simeq 2$ without doing QNMs matching, $v_{\text{com}}^{\text{final}} \simeq 243$ km/s. On the other hand, if we do not include the 2PN correction factor F in Eq. (3) we obtain, again for $\eta = 0.2$, a final recoil $\simeq 135$ km/s at $r \simeq 2$. These results are roughly consistent with the results of Ref. [5], and confirm our diagnostics that the main physical origin of the integrated recoil is the rather well-localized “burst” in linear momentum flux occurring during the plunge.

One might view the large difference between the two models of momentum flux, Eq. (18) versus Eq. (3), in several different ways. One way would be to say that, as we have seen, it is not justified to continue assuming (as is implicitly done in Eq. (3)) the validity of Kepler’s law during the plunge, and therefore that the corresponding prediction for v_{com} is definitely too large¹⁶. On the other hand, we have emphasized above that near the crucial maximum of radiation of linear momentum, the orbital motion becomes mildly relativistic ($\mathbf{p}^2 \sim m^2$, i.e. $(v/c)^2 \sim 0.5$) and, in addition, more complicated than the quasi-circular and quasi-Keplerian cases studied so far in detail in analytical gravitational wave research. Therefore, one might also say that the large difference between the two proposed extrapolations for the momentum flux just reflects our ignorance of what is the correct momentum flux in such a relativistic situation. We do tend to think that our “best bet” estimate, Eq. (60), is probably closer to the truth, but we cannot provide any proof of this belief, nor can we presently define an “error bar” around our preferred estimate (60). One way to estimate an “error bar” around (60) would be to study the effect of using a 3PN-accurate EOB dynamics, and/or to include all the contributions proportional to \dot{R} and \ddot{R} (which were neglected here) in the momentum flux. On the other hand, we consider it likely that the results quoted above (and listed in the last two rows of Table I) coming from the Kepler-law based Eq. (3)

¹⁶ Because, as we have just seen, the known violation of Kepler’s third law, i.e. $K < 1$, is the root of the difference between the two estimates.

furnish an *upper bound* on the correct recoil.

We conclude that none of the current analytical-based estimates of the total recoil are reliable. From Table I, we see that, depending on the analytical representation used for the linear momentum flux during the plunge, we get a final recoil velocity which varies in the range 49 – 172 km/s. This “uncertainty range” in theoretical predictions is illustrated in Fig.9. We view this current theoretical uncertainty as a strong motivation for devoting future work to the specific issue of selecting a reliable¹⁷ analytical model of linear momentum flux during the plunge. There are several avenues one could use towards this aim. One might generalize the work of Ref. [5] by keeping the terms proportional to \dot{r}^2 or p_r^2 , and by making a minimal use of Kepler’s third law¹⁸. Another avenue is to compare analytical and numerical results in the case of a test-particle, $\eta \ll 1$, plunging into a Schwarzschild black hole. One might also try to compare analytic and numerical results in the case of full 3-d simulations of coalescing black holes.¹⁹ However, one should keep in mind that the linear momentum flux is a sub-dominant effect in the gravitational wave emission which can easily get drowned in the “noise” associated, for instance, with the presence of residual incoming radiation in the initial data. Let us note in this respect, that the situation is a priori much better in the (more urgent) problem of the modeling of gravitational radiation (linked to the dominant energy flux) from coalescing black holes. In this case most of the signal-to-noise ratio is linked to the train of waves emitted in the last few orbits before crossing the LSO. The EOB formalism was conceived for dealing with this problem, and the current study should not be interpreted as casting any serious doubt on previous studies [8, 11] which relied mainly on rather robust analytic features of the EOB approach.

¹⁷ By “reliable” we mean here “accurate within 50 %” or so. The current uncertainties in analytical estimates span a factor ~ 5 .

¹⁸ For instance, one might use Kepler’s law only at the level of the derivation of the multipole moments, and not use it anymore when time-differentiating them along plunging orbits. One might also use resummation techniques, notably by using the resummed quasi-Schwarzschild coordinates that enter the EOB formalism.

¹⁹ After the submittal of this paper, remarkable progress in numerical relativity has allowed Baker et al. [45] to report on the first accurate numerical calculation of the recoil velocity of two non-spinning black holes with $\eta = 0.24$. Their result ($v_{\text{recoil}} = 105 \text{ km/s}$) corresponds, if we use the scaling function $\hat{f}(\eta)$, defined after Eq. (60), to a maximum recoil of 161.5km/s. This value falls within the range of analytical estimates summarized in Table I. More precisely, the last row of Table I shows that the momentum flux Eq. (3) predicts a recoil of 110 km/sec when $\eta = 0.24$. We note also that the time evolution, during the coalescence, of the magnitude of the instantaneous recoil velocity showed in Fig. 1 of [45] is in good qualitative agreement with our analytical predictions (see Figs. 5, 8 or 10).

If our ‘best bet’ estimate, Eq. (60), is confirmed, it might have significant astrophysical consequences. For instance, a low value for the terminal recoil will have implications for the formation of massive black holes at high redshifts [43], which may influence various event rates for binaries involving supermassive black holes that LISA may observe. Finally, a recent surge in astrophysical investigations that probe consequences of the recoil indicates that it is desirable to know the dependencies of recoil on the orbital configurations of coalescing black hole binaries [44]. Therefore, it will be also important, in the near future, to extend our approach to the study of the recoil associated with the coalescence of spinning black holes in inspiralling eccentric orbits.

Acknowledgments

We are grateful to Steven Detweiler, Sai Iyer and Kostas Kokkotas for informative communications. AG thanks Gerhard Schäfer for discussions and encouragements. TD thanks the European Research and Training Network ‘Forces Universe’ (contract number MRTN-CT-2004-005104) for partial support. AG gratefully acknowledges the financial support of the Deutsche Forschungsgemeinschaft (DFG) through SFB/TR7 “Gravitationswellenas-
tronomie”. He also thanks IHES for hospitality during early stages of the work.

-
- [1] I. H. Redmount and M. J. Rees, *Comments Astrophys.* **14**, 165 (1989).
 - [2] D. Merritt, M. Milosavljević, M. Favata, S. A. Hughes, and D. E. Holz, *Astrophys. J.* **607**, L9 (2004); P. Madau, and E. Quataert, *Astrophys. J.* **606**, L17 (2004).
 - [3] M. Favata, S. A. Hughes, and D. E. Holz, *Astrophys. J.* **607**, L5 (2004).
 - [4] M. Campanelli, *Class. Quant. Grav.* **22**, S387 (2005)
 - [5] L. Blanchet, M. S. Qusailah, and C. M. Will, *Astrophys. J.* **635**, 508 (2005).
 - [6] M. J. Fitchett, *Mon. Not. R. Astron. Soc.* **203**, 1049 (1983).
 - [7] A. Buonanno, and T. Damour, *Phys. Rev. D* **59**, 084006 (1999).
 - [8] A. Buonanno, and T. Damour, *Phys. Rev. D* **62**, 064015 (2000).
 - [9] T. Damour, P. Jaranowski, and G. Schäfer, *Phys. Rev. D* **62**, 084011 (2000).
 - [10] T. Damour, *Phys. Rev. D* **64**, 124013 (2001).

- [11] A. Buonanno, Y. Chen, and T. Damour, *Transition from inspiral to plunge in precessing binaries of spinning black holes*, gr-qc/0508067, (2005).
- [12] W. Bonnor and M. Rotenberg, Proc. R. Soc. London, Ser. A, **265**, 109 (1961).
- [13] A. Peres, Phys. Rev. **128**, 2471 (1962).
- [14] A. Papapetrou, Ann. Inst. H. Poincaré **14**, 79 (1962).
- [15] K. S. Thorne, Rev. Mod. Phys. **52**, 299 (1980).
- [16] M. J. Fitchett and S. Detweiler, Mon. Not. R. Astron. Soc. **211**, 933 (1984).
- [17] S. Bonazzola, E. Gourgoulhon, P. Grandclément and J. Novak , Phys. Rev. D **70**, 104007 (2004).
- [18] G. Schäfer and A. Gopakumar, Phys. Rev. D **69**, 021501(R) (2004).
- [19] T. Damour, E. Gourgoulhon and P. Grandclément, Phys. Rev. D **66**, 024007 (2002).
- [20] P. Grandclément, E. Gourgoulhon, and S. Bonazzola, Phys. Rev. D **65**, 044020 (2002); E. Gourgoulhon, P. Grandclément and S. Bonazzola, *ibid* **65**, 044021 (2002).
- [21] M. Davis, R. Ruffini, W. H. Press, and R. H. Price, 1971, Phys. Rev. Lett. **27**, 1466 (1971).
- [22] M. Davis, R. Ruffini, and J. Tiomno, 1972, Phys. Rev. D **5**, 2932 (1972).
- [23] W. H. Press, Astrophys. J. **170**, L105 (1971).
- [24] L. Blanchet and T. Damour, Phil. Trans. Roy. Soc. Lond. A **320**, 379 (1986).
- [25] L. Blanchet and T. Damour, Ann. Inst. Henri Poincaré, Phys. Théor. **50**, 377 (1989).
- [26] T. Damour and B. R. Iyer, Ann. Inst. Henri Poincaré, Phys. Théor. **54**, 115 (1991).
- [27] L. Blanchet and T. Damour, Phys. Rev. D **46**, 4304 (1992).
- [28] L. Blanchet, Phys. Rev. D **51**, 2559 (1995).
- [29] L. Blanchet, Class. Quant. Grav. **15**, 1971 (1998).
- [30] L. Blanchet, B. R. Iyer, and B. Joguet, Phys. Rev. D **65**, 064005 (2002).
- [31] L. Blanchet, T. Damour, G. Esposito-Farèse and B. R. Iyer, Phys. Rev. Lett. **93**, 091101 (2004).
- [32] K. G. Arun, L. Blanchet, B. R. Iyer, and M. S. Qusailah, Class. Quant. Grav. **21**, 3771 (2004).
- [33] A. G. Wiseman, Phys. Rev. D **46**, 1517 (1992).
- [34] C. Cutler, L. S. Finn, E. Poisson, and G. J. Sussman, Phys. Rev. D **47**, 1511 (1993)
- [35] W. Junker and G. Schäfer, Mon. Not. R. Astron. Soc. **254**, 146 (1992).
- [36] T. Damour, B. R. Iyer, and B. S. Sathyaprakash, Phys. Rev. D **57**, 885 (1998).

- [37] L. Blanchet, Phys. Rev. D **54**, 1417 (1996); Erratum-ibid. **71**, 129904 (2005).
- [38] T. Damour, B. R. Iyer, and B. S. Sathyaprakash, Phys. Rev. D **62**, 084036 (2000).
- [39] L. Blanchet, T. Damour, B.R. Iyer, C. M. Will and A. G. Wiseman, Phys. Rev. Lett. **74**, 3515 (1995); L. Blanchet, T. Damour, and B. R. Iyer, Phys. Rev. D **51**, 5360 (1995); C. M. Will and A. G. Wiseman, Phys. Rev. D **54**, 4813 (1996). L. Blanchet, B.R. Iyer, C. M. Will and A. G. Wiseman, Class. Quantum Grav. **13**, 575 (1996). L. Blanchet, Phys. Rev. D **54**, 1417 (1996).
- [40] A. Buonanno and T. Damour, *in Proceedings of the MGIXMM Meeting*, Rome, Eds. V. G. Gurzadyan, R. T. Jantzen, and R. Ruffini, World Scientific Publishing, Singapore, **B**, 1637, (2002) (gr-qc/0011052).
- [41] K. D. Kokkotas, and S. Schmidt “Quasi-Normal Modes of Stars and Black Holes”, Living Rev. Relativity 2, (1999), 2. [Online article]
- [42] S. Chandrasekhar and S. Detweiler, Phil. Trans. Roy. Soc. Lond. A **344**, 1639 (1975).
- [43] J. Yoo and J. Miralda-Escude Astrophys. J. **613**, L36 (2004).
- [44] L. Hoffman and A. Loeb, *Three-Body Kick to a Bright Quasar out of Its Galaxy During a Merger*, (astro-ph/0511242); M. G. Haehnelt, M. B. Davies, and M. J. Rees, *Possible evidence for the ejection of a supermassive black hole from an ongoing merger of galaxies* (astro-ph/0511245); D. Merritt, T. S. Bergmann, A. Robinson, D. Batcheldor, D. Axon, and R. C. Fernandes, *The nature of the HE0450-2958 System*, (astro-ph/0511315); N. I. Libeskind, S. Cole, C. S. Frenk, and J. C. Helly, *The Effect of Gravitational Recoil on Black Holes Forming in a Hierarchical Universe*, (astro-ph/0512073).
- [45] J. G. Baker, J. Centrella, D. Choi, M. Koppitz, J. R. van Meter, and M. Coleman Miller, *Getting a kick out of numerical relativity*, (astro-ph/0603204).

TABLE I: Values of $|\mathbf{v}_{\text{com}}|$, $\mathbf{v}_{\text{com}}^x$ and $\mathbf{v}_{\text{com}}^y$, recoil velocity and its x and y components in km s^{-1} for $\eta = 0.2$ at various stages of coalescence for the momentum flux Eq. (18) with different \tilde{F} 's. The last two separated rows (corresponding to $\eta = 0.2$ and $\eta = 0.24$) show the recoil estimates obtained by using, instead of Eq. (18), the (Kepler-law-based) momentum flux Eq. (3).

	$r_{\text{LSO}} \simeq 6.00$	$r_{\text{match}} \simeq 3.00$	$t \rightarrow +\infty$
1.5 PN Taylor \tilde{F}	22.09, 18.05, 12.73	82.84, 51.73, -82.68	72.41, 12.18, -71.37
2 PN Taylor \tilde{F}	22.34, 18.25, 1.29	84.07, 5.23, -83.91	73.52, 12.31, -72.48
$\tilde{F} = 1$	18.50, 15.41, 10.24	59.83, 4.29, -59.67	51.05, 10.29, -50.00
1.5 PN Padé \tilde{F}	20.69, 16.91, 11.92	79.97, 5.11, -79.81	70.19, 11.68, -69.21
2 PN Padé \tilde{F}	16.20, 13.42, 9.08	56.68, 3.96, -56.54	49.02, 9.15, -48.16
Eq. (3), $\eta = 0.2$	23.39, 19.34, 13.16	179.88, 78.54, -161.82	171.55, 136.64, -103.73
Eq. (3), $\eta = 0.24$	15.47, -5.03, -14.62	118.67, -85.74, 82.05	109.64, -103.45, 36.34

TABLE II: Effect of changing the transition point where merger phase goes to QNM ringing on terminal $|\mathbf{v}_{\text{com}}|$ for $\eta = 0.2$ and $\tilde{F} = 1$, when changing the canonical value, $r_{\text{match}} \simeq 3$, by $\pm 20\%$.

	$ \mathbf{v}_{\text{com}} $	$\mathbf{v}_{\text{com}}^x$	$\mathbf{v}_{\text{com}}^y$
$r_{\text{match}} \simeq 3.6$	44.98	-8.05	-44.26
$r_{\text{match}} \simeq 3.00$	51.05	10.29	-50.00
$r_{\text{match}} \simeq 2.4$	58.21	12.60	-56.83

TABLE III: Dependence of scaled terminal recoil velocity $\frac{|\mathbf{v}_{\text{com}}|}{\eta^2 \sqrt{1-4\eta}}$ on η for $r_{\text{match}} \simeq 3.00$ and $\tilde{F} = 1$.

	In km s^{-1}
$\eta = 0.24$	2817.63
$\eta = 0.2$	2853.81
$\eta = 0.1$	2901.29
$\eta = 0.05$	2987.44

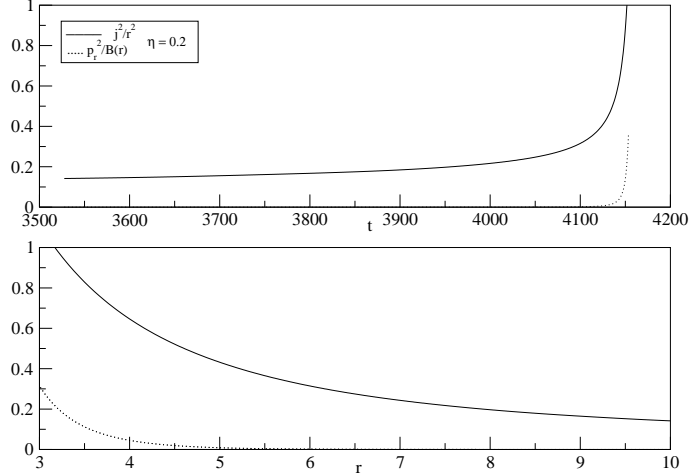


FIG. 1: Plots of ‘azimuthal’ and ‘radial’ kinetic energies as functions of coordinate time t and radial separation r during the late inspiral and plunge for a $\eta = 0.2$ binary. The initial orbital separation, when $t = 0$, was $r = 15$, and the curves were terminated at $t \simeq 4153$, corresponding to $r = 3$. The plots show that $j(t)^2/r^2$ dominates $p_r(t)^2/B(r)$ during the entire EOB evolution, including the plunge (down to $r = 3$).

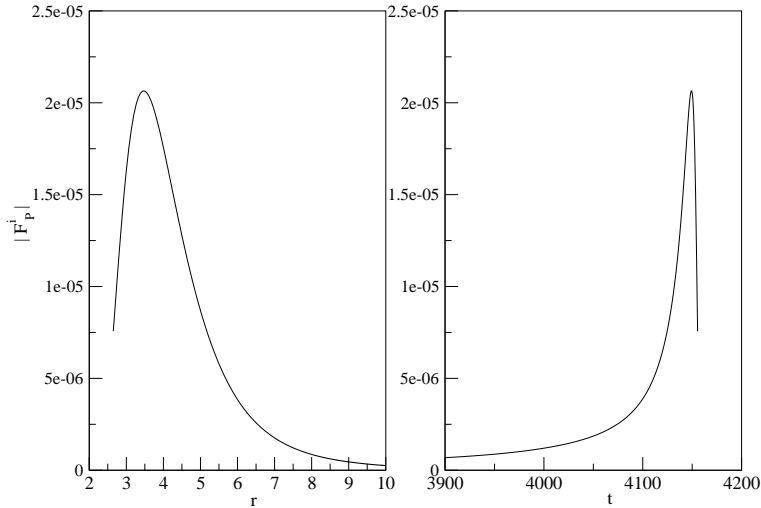


FIG. 2: Magnitude of the linear momentum flux (in the quasi-Newtonian approximation) as a function of r (left panel) and t (right panel) during the late inspiral and plunge for a $\eta = 0.2$ binary, whose initial orbital separation, when $t = 0$, was $r = 15$. We terminated the plunge arbitrarily around $r \simeq 2.65$.

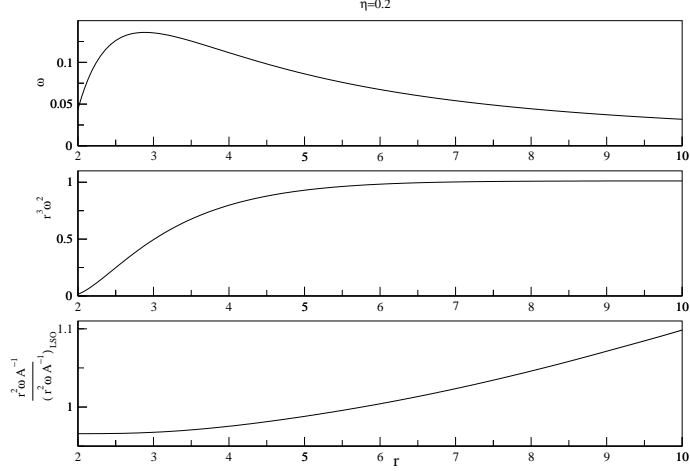


FIG. 3: Plots of ω , $r^3\omega^2$ and $\frac{r^2\omega A^{-1}}{(r^2\omega A^{-1})_{\text{LSO}}}$ in terms of r resulting from the EOB evolution, given by Eqs. (17), for $\eta = 0.2$ binary. The panels clearly demonstrate that the orbital frequency evolves differently during the late inspiral and the subsequent plunge. Note in particular the strong decrease of the “Kepler combination” $K \equiv r^3\omega^2$ during the plunge.

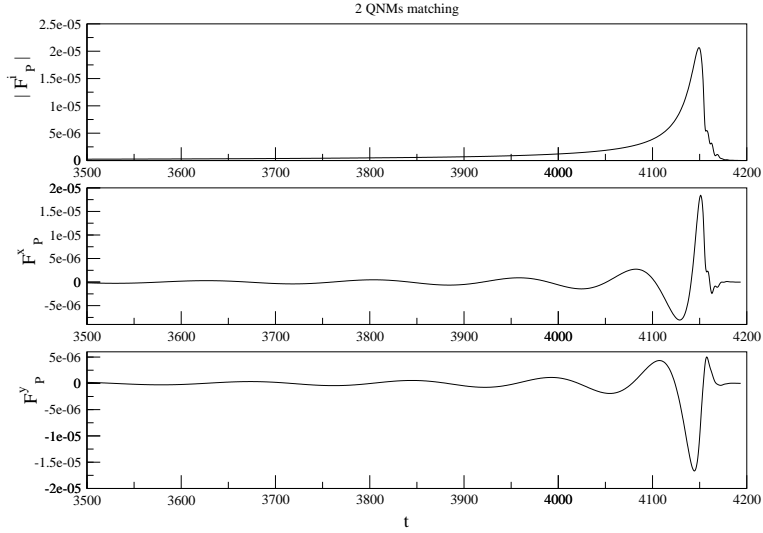


FIG. 4: Plots for the magnitude, x and y components of the linear momentum flux (quasi-Newtonian approximation) versus t during the coalescence of a binary with $\eta = 0.2$. For this figure, the ring-down phase is described by 2 QNMs and orbital separation of the binary, when the numerical evolution began, was $r = 15$.

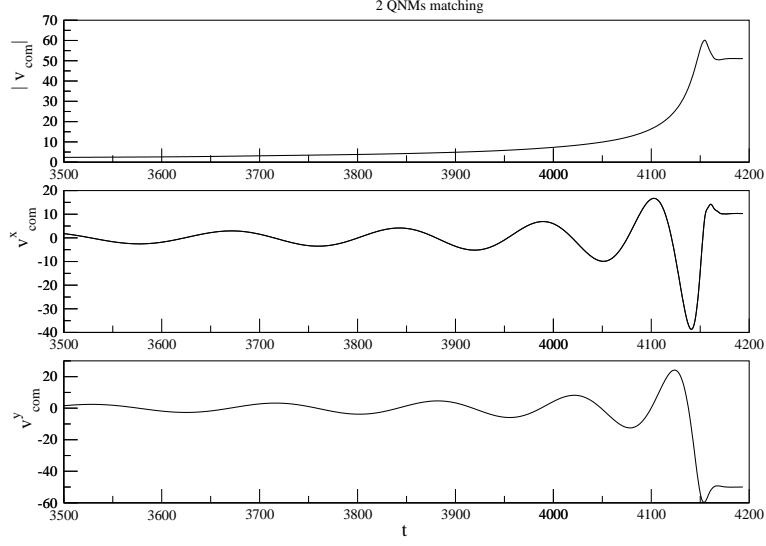


FIG. 5: Temporal plots for the magnitude, x and y components of recoil velocity for the binary configuration described in Fig. 4 ($\eta = 0.2$, quasi-Newtonian flux, 2 QNM's).

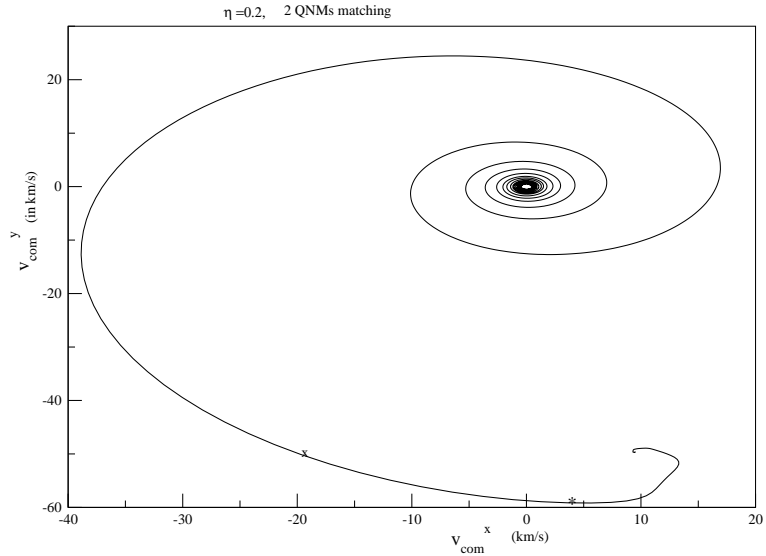


FIG. 6: Parametric plot of v_{com}^x versus v_{com}^y during the coalescence of a $\eta = 0.2$ binary. We employ the quasi-Newtonian approximation to the linear momentum flux followed by a 2 QNMs description of the ring-down phase. The symbols \times and $*$ respectively indicate the positions where the linear momentum flux reached its maximum value and where matching to the ring-down phase was done. The initial orbital separation of the binary, when $t = 0$, was $r = 15$.

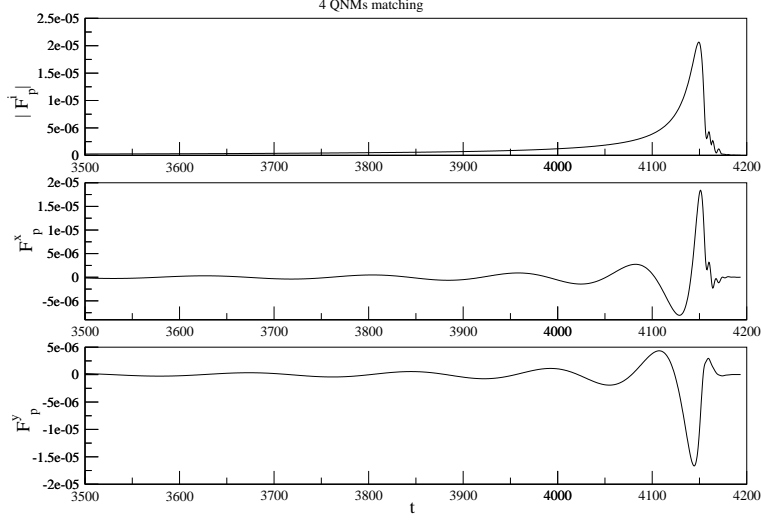


FIG. 7: Plots for the magnitude, x and y components of the quasi-Newtonian linear momentum flux versus t during the coalescence of a binary with $\eta = 0.2$. In this case, the ring-down phase is described by 4 QNMs and the initial orbital separation of the binary, when $t = 0$, was $r = 15$.

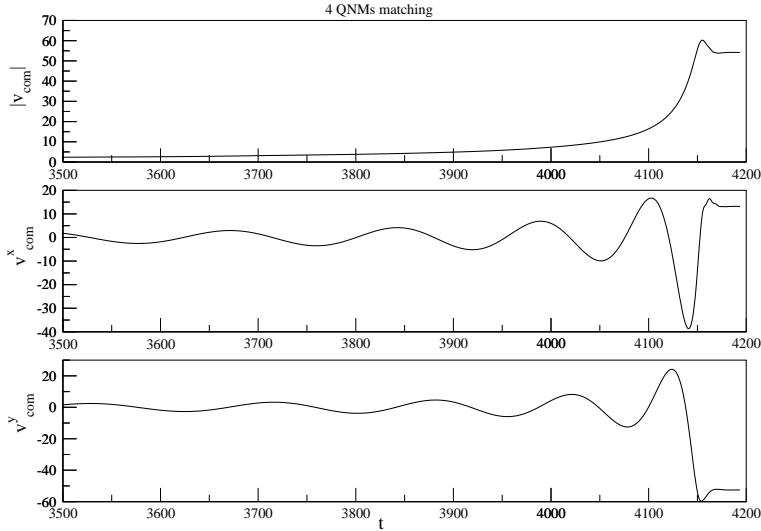


FIG. 8: Temporal plots for the magnitude, x and y components of recoil velocity for the binary configuration described in Fig. 7 ($\eta = 0.2$, quasi-Newtonian flux, 4 QNM's).

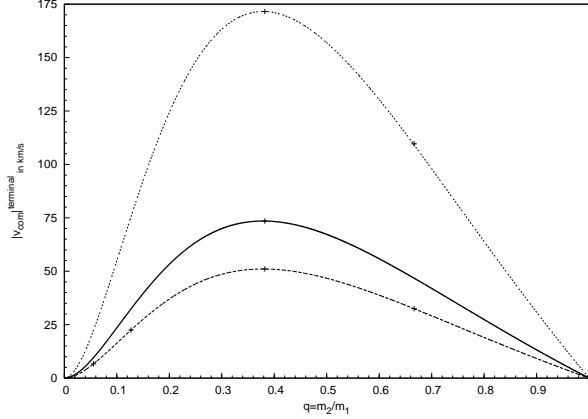


FIG. 9: Our ‘best-bet’ estimate (solid line) for the terminal recoil as a function of the mass ratio $q = \frac{m_2}{m_1}$ based on Eq. (60) with $\tilde{F} = 1.35$, corresponding to using the 2PN, Taylor \tilde{F} in the momentum flux expression Eq. (18). The “theoretical uncertainty” around this best-bet estimate is illustrated by plotting the results of using: (i) a quasi-Newtonian flux (Eq. (18) with $\tilde{F} = 1$) [dot-dashed lower curve], or (ii) the Kepler-law-based 2PN flux Eq. (3) [dotted upper curve]. The estimates taken from Tables I and III are denoted by + symbols.

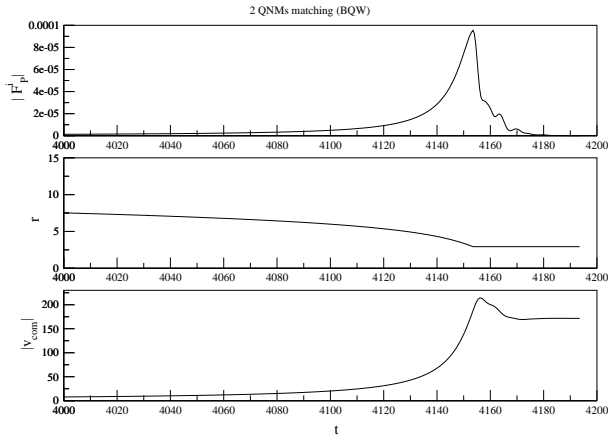


FIG. 10: Temporal plots, along the EOB evolution, for the magnitude of the “Blanchet-Qusailah-Will” linear momentum flux, defined by Eq. (3), the orbital separation r and the associated recoil $|v_{\text{com}}|$ in km/s for $\eta = 0.2$ binary. We terminate the plunge around $r \simeq 3$ and perform two QNMs matching for the ring-down phase. [In Ref. [5] the evolution was formally continued down to $r \simeq 2$].